UNCLASSIFIED CONFIDENTIAL

Copy 601
NASA TM X-518

NASA TM X-518

0063 12563
code-1

TECHNICAL MEMORANDUM

X-518

LANDING-GEAR BEHAVIOR DURING TOUCHDOWN AND RUNOUT FOR 17 LANDINGS OF THE X-15 RESEARCH AIRPLANE

By James M. McKay and Betty J. Scott

Flight Research Center
Edwards, Calif.

OTS PRICE

XEROX $

MICROFILM $

CLASSIFICATION CHANGED TO
UNCLASSIFIED
AUTHORITY NASA LIST #1, Dec 1, 1962
By

DECLASSIFIED DOCUMENT - SUBJECT TO RESTRICTIONS

This material contains information affecting the national defense of the United States within the meaning of the espionage laws, Title 18, U.S.C., Secs. 793 and 794, the transmission or revelation of which in any manner to an unauthorized person is prohibited by law.

NATIONAL AERONAUTICS AND SPACE ADMINISTRATION
WASHINGTON March 1961

CONFIDENTIAL

UNCLASSIFIED

CONFIDENTIAL

NATIONAL AERONAUTICS AND SPACE ADMINISTRATION

TECHNICAL MEMORANDUM X-518

LANDING-GEAR BEHAVIOR DURING TOUCHDOWN AND RUNOUT FOR 17 LANDINGS OF THE X-15 RESEARCH AIRPLANE*

By James M. McKay and Betty J. Scott

SUMMARY

Data are presented for the pretouchdown condition, the impact period, and the runout phase of 17 landings made with the X-15 airplane. Vertical velocities up to 9.5 feet per second and true ground speeds between 145 knots and 238 knots were recorded during the landings.

The results of the investigation indicate that the highest main-gear shock-strut force, drag reaction, airplane upper-mass response, and horizontal-tail load occurred during the nose-gear touchdown for all of the landings.

The mean value of the coefficient of friction of the main-gear skids calculated for one landing was 0.33. The combined effect of the high skid drag and low rolling friction of the nosewheel tires provided more than adequate directional stability during the runout. As a consequence, pilot-induced inputs resulted in only small changes to the airplane direction of motion during the runout.

No nosewheel shimmy was observed in any of the landings, despite the absence of a shimmy damper.

INTRODUCTION

The approach and landing operation of unpowered rocket airplanes has always required considerable pilot concentration, but has usually been accomplished with a relatively conventional procedure. The X-15 airplane initiates a class of vehicles--manned, boost glide, and maneuverable reentry--that requires a landing-gear system designed to expend a minimum of airplane space and weight, withstand the high temperatures resulting from aerodynamic heating, be capable of sustaining high landing speeds, and provide satisfactory directional

*Title, Unclassified.

CONFIDENTIAL

UNCLASSIFIED

stability during the runout phase of the landing. The configuration chosen for the X-15 airplane to meet these requirements consists of a skid-type main gear located well to the rear of the airplane center of gravity and a conventional dual-wheel nose gear located well forward of the center of gravity.

In order to investigate the characteristics of such a landing-gear system, the gear and the airplane upper mass of two X-15 airplanes were instrumented by the NASA Flight Research Center, Edwards, Calif., and North American Aviation, Inc., to measure pertinent quantities during the landing.

SYMBOLS

a_l center-of-gravity longitudinal acceleration, g units

a_n center-of-gravity vertical acceleration, g units

a_v main-gear and nose-gear upper-mass vertical acceleration, g units

C_D airplane drag coefficient, corresponding to full flaps and speed brakes and extended landing gear

D_A airplane aerodynamic drag, $C_D qS$, lb

F_h drag ground reaction, lb

F_s shock-strut force, lb

F_t horizontal-tail aerodynamic load, lb

F_v vertical ground reaction, lb

g acceleration due to gravity, ft/sec^2

q pitching velocity, radians/sec

q dynamic pressure, lb/sq ft

S wing area, sq ft

Δt_n time interval between initial main-gear contact and nose-gear contact, sec

V true ground velocity, knots

V_v vertical velocity, ft/sec

W_L airplane weight at landing, lb

α indicated angle of attack, deg

δ_h horizontal-tail deflection, deg

δ_s shock-strut displacement, in.

μ coefficient of friction

Subscripts:

m main gear

n nose gear

AIRPLANE

The X-15 airplane (figs. 1 and 2) is a rocket-powered research aircraft designed to attain speeds up to 6,600 feet per second or altitudes up to 250,000 feet. The lift-drag ratio in the landing configuration is about 3.5. The airplane's control system incorporates an all-movable and differentially operated horizontal tail for pitch and roll motion and a vertical tail consisting of a fixed portion and an all-movable portion for yaw control. The all-movable section of the lower vertical tail is jettisoned just prior to touchdown to allow for ground clearance.

The airplane was designed by North American Aviation, Inc., through the cooperative effort of the U.S. Air Force, the U.S. Navy, and the National Aeronautics and Space Administration. Physical characteristics of the airplane are given in table I.

LANDING-GEAR SYSTEM

The landing-gear system of the X-15 consists of a nonsteerable, full-castering dual-wheel nose gear located 23.3 feet forward of the airplane center of gravity (landing condition) and a skid-type main gear located under the tail 15.8 feet rearward of the center of gravity.

UNCLASSIFIED

Main Gear

The main-gear legs are Inconel X struts attached to the fuselage by trunnion fittings (figs. 3(a) and 3(b)) and through bell-crank arms to high-pressure shock struts installed inside the fuselage. The two 6-inch-wide, 3-foot-long skids, fabricated from 4130 steel, are universally mounted to the struts to allow for pitching and rolling motion, but are restrained for parallel alinement. The drag braces are attached to the fuselage by semiuniversal fittings and, similarly, connect with the skids ahead of the strut-attachment pin. Bungee-type springs connect the leading edge of the skid to the main-landing-gear leg to insure nose-up attitude of the skids prior to touchdown.

In the retracted position the landing-gear legs are folded forward against the outside of the fuselage, and the skids are stored with their rear portion overlapping the landing-gear leg. After release, the gear is extended down and rearward by gravity and airloads.

Since the engine and its accessories limit the size of the landing-gear components mounted in the fuselage, the shock-strut was designed with a minimum of stroke. The shock strut is of the oleopneumatic type with a pressure-relief valve and a metering pin acting in parallel to create the hydraulic load. During the main-gear phase of the landing, the hydraulic load is created by the metering pin. When the total stroke is one-half complete, the metering pin closes off the orifice and the hydraulic load is provided by the relief valve for the remainder of the stroke. With the relief valve open, the shock-strut force is a function of piston position; the total reaction is the sum of the hydraulic and airspring force. The relief valve provides for an essentially constant pressure drop and allows for a free flow for fast extension during rebound.

The strut-airspring characteristic is a function of the air pressure and the quantity of oil pumped into the strut in its fully extended position. With the strut fully compressed, the air pressure is sufficient to restore the strut to its normal static height. The strut-inflation pressures are given in table II for each flight of the airplane.

The initial landings (one with the X-15 number 1 airplane and three with the X-15 number 2) indicated that additional energy-absorbing ability was required for the main-gear system for landing weights up to 14,500 pounds. To meet this requirement, the maximum shock-strut stroke was increased from 2.58 inches to 3.58 inches. The remainder of the flights were made with the redesigned shock strut. The increase in maximum stroke made it necessary to add 4 inches to each main-gear leg for ground clearance of the unjettisonable portion of the lower vertical fin with the shock struts fully compressed.

Nose Gear

The nose gear (fig. 4) is of conventional design, nonsteerable, with full 360° castering in the deflected condition. Dual corotating wheels are utilized for prevention of shimmy and also for low castering resistance to provide satisfactory directional stability during the runout. In order to insure proper wheel alinement prior to touchdown, the nose gear is restrained in the fully extended position. The shock strut was designed with a total travel of 18 inches and a nominal design strut-inflation pressure of 184 psi in the fully extended position. The VII-type nose-gear tires are 18 inches × 4.4 inches in size with a rating of 8 ply. The tires are inflated to a pressure of 185 psi and have a rolling radius of 8 inches at this pressure. In order to retract the nose gear in a minimum of space during flight, the shock strut is compressed and is held in this position by a lock arrangement that is automatically released when the gear extends (fig. 4). Aerodynamic heating of the pneumatic tires and oleopneumatic shock strut is kept to a minimum by insulation of the storage compartment.

The initial landings of the airplane indicated a rebounding of the nosewheels on the lakebed following the spin-up period. As an illustration of the nose-gear rebound, the discontinuity of the nosewheel track is shown in figure 5. Examination of the system showed that violent mixing of the air and fluid occurred, which resulted in foaming of the fluid. Insufficient time elapsed between landing-gear extension and touchdown to allow this foam to dissipate. Consequently, there was a decreased hydraulic resistance at the beginning of the stroke, which resulted in lower energy-absorbing ability of the strut. The foaming was largely eliminated by adjusting the strut airspring in the stored position to just enough pressure to elongate the strut during extension, and by increasing this pressure after extension to its normal value of 184 psi. The strut was pressurized by using an external nitrogen bottle mounted in the nose-gear compartment and actuated during release. In order to check the operation of this system, the nose-gear strut pressures were measured immediately after each landing.

INSTRUMENTATION

The quantities measured during the approach, touchdown, and runout phases of the landings are given in the following tabulation:

UNCLASSIFIED

Airplane	Main gear	Nose gear
Center-of-gravity vertical acceleration	Shock-strut force	Vertical ground reaction[1]
Airspeed	Drag ground reaction[1]	Drag ground reaction[1]
Angle of attack	Shock-strut deflection	Shock-strut deflection
Pitching velocity	Upper-mass vertical acceleration	Upper-mass vertical acceleration
Rolling velocity		
Sideslip angle		
Flap angle		
Horizontal-tail load		
Horizontal-tail angle		

[1]Not recorded with the X-15 number 1 airplane.

Airspeed was measured with an NASA pitot-static tube mounted on the end of the nose boom. Free-floating vanes, also mounted on the nose boom, were used to measure angles of attack and sideslip.

Akeley phototheodolite cameras, running at 19 frames per second, tracked the airplane from a height of approximately 80 feet above the runway through touchdown and final landing runout. From this photographic coverage, such information as landing coordinates, airplane altitude, flight-path velocity, and vertical velocity at landing was obtained.

The location of some of the main-landing-gear instrumentation is shown in figure 3(a). Strain gages were mounted on the upper and lower surfaces of each of the bell-crank arms and were arranged to measure the axial force applied to the shock-strut cylinder. The strain gages mounted on each main-gear drag brace were arranged to measure tension loads in the drag brace resulting from the drag force acting on the skids. Strain gages mounted on both the left and right spindles of the all-movable horizontal tail were located in a vertical plane to measure the bending moment, torque, and shear resulting from the load normal to the tail. Strain gages were mounted on the nose-gear trunnion and down-lock mechanism to measure the vertical loads and drag loads at the nose-gear axle.

The airplane center-of-gravity acceleration was measured by means of a vane-type, magnetically damped three-component accelerometer with a natural frequency of 32 cycles per second. Linear strain-gage accelerometers were located at the airplane center of gravity, directly above each main gear, and at the nose gear to measure vertical accelerations. The natural frequency of the strain-gage accelerometers was greater than 125 cycles per second. The recording galvanometers had a natural frequency of about 100 cycles per second.

Shock-strut displacement for the left and right main gear and the nose gear was measured by strut-position transmitters. The transmitters consisted of a circular-type potentiometer connected between the upper and lower sections of each shock strut by lightweight levers to conform with the scissors principle during strut displacement. A typical installation is shown in figure 4 for the nose gear.

All strain-gage, accelerometer, and shock-strut-displacement outputs were recorded on photographically recording oscillographs and were synchronized by a common timer.

CALIBRATION AND DATA REDUCTION

The acceleration at the airplane center of gravity presented as data prior to touchdown was measured by the three-component accelerometer. The accelerations at the center of gravity, as well as at the nose-gear and main-gear upper mass, during the landing impact and runout were measured by the linear strain-gage accelerometers.

For each main gear, the bell-crank-arm strain gages were calibrated to give the axial load on the shock-strut cylinder. The strain gages on the left and right main-gear drag braces were calibrated to give the drag-brace tension loads resulting from the drag loads on the skids. From the geometry of the main-gear system, the drag-brace tension loads were used to calculate the drag reaction between the skids and the ground. No interaction exists between the drag-brace load and the main-gear shock strut, since pivot points at the fuselage for the drag brace and the landing-gear leg fall on a line that is essentially parallel to the longitudinal centerline of the fuselage.

The strain gages on the left and right horizontal-tail spindles were calibrated to measure shear, bending moment, and torque at the root station. Equations, which accounted for the interaction of the bending and shear gages, were used to calculate the load normal to the horizontal tail and were developed according to the method of reference 1. The aerodynamic load was obtained by adding inertia corrections to the measured forces. The inertia term was the product of the mass outboard of the spindle strain-gage stations (horizontal-tail panel) and the normal acceleration at the tail of the airplane.

The nose-gear structure of the X-15 number 2 airplane was used as a strain-gage balance to measure vertical and drag forces on the axle. The relationship between the strain-gage response and the applied load was determined by calibrating the nose gear in a load-testing machine at North American Aviation, Inc. The gages were calibrated for trunnion vertical reactions and trunnion drag and down-lock drag reactions. The

UNCLASSIFIED

gages were also calibrated to determine the effects of side load at the axle and to establish the interaction (for example, the effects of drag forces on the vertical shear gages) under various combinations of vertical, drag, and side load.

In order to determine if fuselage deflections during the landing touchdown induced axial compression loads in the nose-gear trunnion which would interact with the drag gages, two additional gages were installed and calibrated to measure the axial load in the trunnion. The calibration showed that these loads had a negligible effect.

The nose-gear ground-reaction forces, both vertical and drag, are considered to be the loads at the nosewheel axle; no corrections are included for the inertia forces of the nose-gear lower mass (approx. 94 lb).

LANDING CONDITIONS

The landings of the X-15 airplanes reported herein (table III) were made on designated, marked strips on the hard surface of Rogers Dry Lake at Edwards Air Force Base, Calif., with the exception of one emergency landing on an alternate landing site, Rosamond Dry Lake. The landings, which were made following general research flights of the X-15 airplane, resulted in vertical velocities at main-gear touchdown ranging from about 1.0 to 9.5 feet per second and true ground speeds between 145 knots and 238 knots. The true ground speed at touchdown was calculated by using the interval between the time the main gear and the nose gear initially touched the ground (as obtained from oscillograph records) and the measured distance between the main-gear- and nose-gear-touchdown points on the lakebed. The angles of attack at touchdown ranged from 4.7° to 11.2°. The maximum wind velocity across the lakebed for any of the landings was approximately 20 knots.

The X-15 airplanes used in the landings reported herein were flown by three experimental test pilots, designated A, B, and C (table III). Pilots A and B had considerable experience with rocket research aircraft, and each of the three pilots had performed numerous landings using operational aircraft modified to simulate X-15 characteristics (ref. 2).

Escort pilots in operational airplanes accompanied the X-15 through the approach and touchdown on the lakebed and informed the pilot of airspeed and altitude.

PRESENTATION OF RESULTS

The flight-designation system (tables II and III) which has been established for the X-15 research program consists of three terms: The first term indicates the X-15 airplane by number; the second term indicates the free-flight number of that airplane; and, the third term indicates the number of airborne X-15/B-52 missions for a given X-15 airplane. For example, the flight designated as 1-3-8 was made with the number 1 airplane and was the third free-flight and the eighth airborne mission of this airplane.

As stated previously, the initial landings of the X-15 airplane (flights 1-1-5, 2-1-3, 2-2-6, and 2-3-9) were made with the original main-landing-gear system.

A summary of the maximum measured quantities for the main-gear touchdown, nose-gear touchdown, and runout is given in table II. Pretouchdown conditions of the X-15 number 1 and number 2 airplanes just prior to ground contact are given in table III. The landing weights and vertical velocities are shown in table II and table III for convenience in comparing results. Some data previously reported in reference 3 for the landing following flight 1-1-5 and in reference 4 for the landing following flight 2-1-3 have been corrected as a result of more reliable methods of data reduction. The true ground speed for the landing following flight 1-1-5 is 168 knots instead of 158 knots, and the nose-gear vertical velocity at touchdown is 17.4 feet per second instead of 13.5 feet per second, as shown in reference 3. For the landing following flight 2-1-3 (ref. 4), the nose-gear vertical velocity at touchdown is 13.2 feet per second instead of 15.0 feet per second.

Some of the nose-gear shock-strut pressures measured immediately after each landing varied slightly from the nominal value of 184 psi because of leakage and temperature effects. The pressure for the landing following flight 2-5-2 (330 psi) was the result of overpressurization during servicing.

Typical time histories of shock-strut force, shock-strut displacement, and upper-mass acceleration for the present gear system are shown in figures 6(a) to 6(d) for the X-15 number 1 airplane from 0.2 second prior to contact with the lakebed through the main-gear- and nose-gear-touchdown period. Similar quantities, as well as main-gear and nose-gear drag reaction and nose-gear vertical reaction, are presented in figures 7(a) to 7(d) for the X-15 number 2 airplane. Instrument malfunction during some of the landings resulted in some unreliable data. For example, in figure 7(d) no drag-reaction data were obtained for the left main gear or for the nose gear, and in figure 7(b) the measured nose-gear drag reactions prior to touchdown were too high

UNCLASSIFIED

in magnitude to be considered as aerodynamic drag. However, the incremental values of nose-gear drag reactions are considered satisfactory.

Such quantities as angle of attack, pitching velocity, center-of-gravity vertical acceleration, horizontal-tail deflection, and horizontal-tail load are shown in figures 8(a) to 8(d) and figures 9(a) to 9(d) for the X-15 number 1 and number 2 airplanes, respectively. A photograph illustrating typical main-landing-gear-skid marks on the lakebed is shown in figure 10(a), and landing-gear tracks during runout as obtained from measurements on the lakebed are shown in figures 10(b) and 10(c). A photograph of landing-gear marks during the runout phase of a typical landing is shown in figure 11. The variation of coefficient of friction and true ground speed for the main-gear skids is shown in figures 12(a) and 12(b) for the runout phase of one landing.

DISCUSSION

The main-gear system located under the tail of the X-15 airplane results in a landing-impact maneuver different from that experienced on aircraft with a conventionally placed gear. A schematic illustration of the touchdown is shown in figure 13. Prior to touchdown, negative horizontal-tail deflections established the nose-high attitude during the landing flare (fig. 13(a)). After initial impact, rotation of the airplane about the main gear occurs, and the airplane essentially "slams" down onto its nose gear (figs. 13(b) to 13(d)). A second impact then occurs on the main gear as the result of rotation about the nose gear (fig. 13(e)). The gear system is then restored to its normal static height for the runout (fig. 13(f)). A more complete discussion of the effect of the location of the rear landing gear on landing behavior is given in reference 5.

Pretouchdown Conditions

The airplane attitude just prior to touchdown for a typical landing is shown in figure 14. For all the landings reported herein, the vertical velocities at main-gear touchdown ranged from 1.0 to 9.5 feet per second; the latter velocity, occurred during the emergency landing on Rosamond Dry Lake (flight 2-3-9). The angles of attack at touchdown ranged from 4.7°, at which the indicated airspeed at touchdown was the greatest (214 knots), to 11.2°, at which the indicated airspeed was 160 knots. The lowest indicated airspeed (153 knots) at touchdown occurred on the first landing of the X-15 airplane (flight 1-1-5) during which severe longitudinal oscillations were encountered just prior to touchdown (ref. 6). The instantaneous airplane lift at touchdown, presented as

center-of-gravity acceleration just prior to first skid contact, varied from 85 percent to 140 percent of the airplane landing weight. There appeared to be no consistent effect of lift on vertical velocity at initial touchdown.

Main-Gear Touchdown

Figures 6 and 7 present typical measured quantities from four landings of each X-15 airplane. The data are presented from initial touchdown; zero time coincides with the time of the first contact of a skid trailing edge with the lakebed. The time from the initial to the second skid contact was the result of one or more factors, including airplane roll attitude and main-landing-gear-skid inclination. The data show that this time interval was small, with a maximum of 0.20 second experienced during the landing following flights 1-3-8 and 1-7-12.

The similarity of shock-strut force, shock-strut displacement, and upper-mass acceleration between the left and right gear during the main-gear impact is shown in figures 6 and 7. The landings, in which both main gears equally absorbed the landing-impact energy, were typical of most of the landings; however, two exceptions were experienced following flight 1-3-8 (fig. 6(b)) and flight 2-2-6 (fig. 7(a)). For all the landings both the left and the right skid were solidly on the lakebed and had completed their respective landing impact before nose-gear touchdown occurred. Table II indicates that, for all of the landings, only 5 to 58 percent of the total shock-strut stroke of each main gear was used for the initial impact. In all landings with the redesigned main-gear system, sufficient stroke remained for the main-gear system to absorb the energy which was transmitted to the main gear after nose-gear impact.

A photograph of main-gear-skid marks on the lakebed for the landing following flight 2-4-11, for which the vertical velocity at touchdown was 6.5 feet per second, is shown in figure 10(a). Measurements of the main-gear tread for this landing, that is, the distance between the centerline of the left and right skid marks, are shown in figure 10(b) for the impact period. Also shown for comparison (fig. 10(c)) are the tread measurements for the landing following flight 1-6-11, for which the vertical velocity at touchdown was 1.0 feet per second. The figure shows that for the higher vertical velocity the skids made solid contact and stayed on the lakebed almost immediately after the trailing edge of each skid initially scuffed the surface.

UNCLASSIFIED

Rotation About Main Gear

Once the initial main-gear impact has been made, the main-gear system encounters several sizable increases in load. During rotation, the airplane is losing lift, thus increasing the load on the main gear and, consequently, increasing the shock-strut displacement. As the vertical velocity of the main-gear upper mass approaches zero, the angle of the horizontal tail with respect to the free-stream flow is increased (fig. 13). This angle further increases as the airplane rotates to a negative attitude at nose-gear contact, resulting in an increase in horizontal-tail load. The records show also that the horizontal-tail angle steadily increases in a negative direction during the landing due to control inputs. The loads resulting from the high angle of attack of the tail increase the main-gear loads, since the main gear is located close to the forward and rearward center of pressure of the horizontal tail. The direction of all the loads--the down load on the tail, the negative wing lift, and the airplane inertia loads--results in high values of the main-gear reaction during this portion of the landing. As can be seen in figures 6 and 7, airplane rotation onto the nose gear appreciably increased the main-gear shock-strut force, drag ground reaction, and upper-mass response over the values experienced during the main-gear phase of the landing. Also, the highest values of center-of-gravity vertical acceleration occurred during the nose-gear touchdown.

The data of figures 8 and 9 illustrate the variation of airplane angle of attack and pitching velocity with time during the landing period. The angle-of-attack data presented are indicated values and have not been corrected for pitching velocity. Because of the rearward location of the main gear, the pitching velocities at nose-gear touchdown are of high magnitudes, with a maximum of 0.445 radian per second.

Figures 10(b) and 10(c) show that, as the airplane rotated, the maximum main-gear tread was reached shortly after nose-gear contact, indicating that the maximum vertical reaction on the main-gear system occurred in this area. Comparison of the landings following flights 2-4-11 and 1-6-11 shows that the shorter distance and, also, the smaller interval of time for the nose gear to contact the lakebed can be related to such factors as lower angle of attack and higher vertical velocity during the main-gear touchdown.

The time histories of figure 7 show that the nose-gear vertical reaction reached an initial peak 0.05 second to 0.07 second after the start of the nose-gear impact, which was the end of the spin-up period. A second peak occurred about 0.18 second after nose-gear impact following the springback period. For most of the landings in which the nose-gear vertical and drag reactions were measured, the maximum vertical reaction was reached at the end of the spin-up period.

Figure 15 compares the X-15 touchdown vertical-velocity and angle-of-attack design limits with similar data obtained from actual landings for the original gear system and for the system now in use. As a result of the modifications to the main-gear system discussed previously, the allowable angle of attack at touchdown was extended, as indicated by the dashed line. The solid symbols indicate the landings that were made with the original gear system. It will be noted that the most severe landing (flight 2-3-9) was made outside of the present gear envelope.

Coefficient of Friction of Main-Gear Skids

The coefficient of friction was calculated (see appendix) for both the left and right main skids and is shown in figure 12(a), along with the results obtained by using the total main-gear drag and vertical skid forces, for a true ground speed from 184 knots to the end of the landing runout. The touchdown velocity for this landing was 198 knots true ground speed.

The coefficient of friction immediately after nose-gear touchdown is of the order of 0.35 for the main-gear skids, after which the values appear to decrease somewhat with decreasing ground speed. The trend of decreasing coefficient of friction is evident to about 50 knots, corresponding to the velocity at which the coefficient of friction would begin to increase to its maximum value (impending friction) at the end of the runout. These values agree satisfactorily with the results, shown in figure 12(b), obtained by using an alternate method and appear to be similar up to the maximum ground speed of 103 knots, which was used in the alternate method. Results from some X-15 lakebed trailer tests, in which the skid coefficient of friction at 61 knots was 0.35, compare favorably with the values from the actual landing runout (fig. 12(a)). For both methods, the mean value of the coefficient was 0.33.

Nosewheel Shimmy

In figure 11 the absence of nosewheel shimmy is illustrated by the straight tire marks following the nose-gear touchdown. No nosewheel shimmy was observed in any of the landings. Tests made previously by the National Aeronautics and Space Administration on the landing track at Langley Research Center during some high-speed ground runs with the X-15 nose gear without a shimmy damper had indicated the absence of shimmy. As a result, the damper was removed prior to the first flight of the X-15 airplane.

UNCLASSIFIED

Directional Stability

Figure 11 also illustrates the runout phase of a typical landing during which no attempt was made to steer the airplane after touchdown. This landing was made into a head wind estimated to be between 3 to 5 knots. The figure illustrates the ability of the landing-gear system to provide satisfactory directional stability during the runout by action of the low rolling friction of the nosewheels in combination with the high drag forces on the main-gear skids. Landings during which attempts were made to steer the X-15 airplane after touchdown show that rudder input has little or no effect on altering the direction of motion. Because the nose-gear wheels are continuously alining themselves with the airplane direction of motion, and because the coefficient of friction of the main-gear skids in a side direction is similar to that in a drag direction, rudder input alone simply yaws the airplane. Roll input appears to be more effective than rudder input for altering the direction of motion, since the vertical ground reaction is increased on one skid. The effects are small, however, and surveys of some landing runouts showed that, although full control deflection was used, the maximum lateral displacement on the lakebed was only 523 feet in a runout distance of 6,073 feet. Results of the survey also showed that pilot inputs for controlled changes in airplane direction must be induced immediately after touchdown.

CONCLUSIONS

This paper presents some results of an analysis of landing-gear behavior and airplane-response characteristics made during 17 landings of the X-15 research airplane. The data were obtained at vertical velocities up to 9.5 feet per second and forward ground speeds from 145 to 238 knots. A summary of the principal conclusions follows:

1. The highest values of main-gear shock-strut force, drag reaction, and response of the airplane upper mass occurred after the nose-gear touchdown.

2. Horizontal-tail loads increased the main-gear vertical reaction and reached a maximum value during the nose-gear touchdown.

3. Nosewheel shimmy was not observed on any of the landings during the touchdown and runout phase, despite the absence of a nose-gear shimmy damper.

4. The low rolling friction of the nosewheels, in combination with the high drag forces on the main-gear skids far to the rear of the center of gravity, provides satisfactory directional stability during the runout phase of the landing.

5. Landing results from the X-15 airplane have indicated that roll input is more effective than rudder input alone in altering the airplane direction of motion during the runout. The effects, however, are small, and the control inputs must be induced immediately after landing.

6. The mean value of the coefficient of friction for the main-gear skids calculated for one landing runout was 0.33. This compared favorably with results obtained from lakebed trailer tests at 61 knots true ground speed.

Flight Research Center,
National Aeronautics and Space Administration,
Edwards, Calif., January 10, 1961.

UNCLASSIFIED

APPENDIX

METHOD OF COMPUTING COEFFICIENT OF FRICTION OF MAIN-LANDING-GEAR SKIDS DURING A RUNOUT

During the runout phase of some of the landings, data were collected which permitted an analysis of the coefficient of friction between the main-gear skids and the dry lakebed. The landing runout following flight 2-8-16 was chosen for this analysis, and that part of the runout which occurred between nosewheel touchdown and the end of the landing run was used. The data from the landing run showed only slight effects on longitudinal and vertical accelerations as a result of ground roughness. Roll motion through the runout was small, and a steering attempt caused the airplane to terminate the runout in a gradual left turn. This resulted in a slightly higher vertical reaction on the left main-gear skid than on the right skid. The analysis was made on the basis of the following simple relation for the skid coefficient of friction

$$\mu_m = \frac{F_{h_m}}{F_{v_m}}$$

The values of F_{h_m} and F_{v_m} were determined from data recorded for each main-gear skid during the runout. The geometry of the main-gear system allowed the drag-brace loads to be resolved to the drag force F_{h_m} between the skids and the ground. Since slight pitching, vertical, and rolling motions were encountered during the runout, the main-gear shock-strut reaction to the skid vertical load was regarded as equal to the strut airspring force; that is, the airplane was essentially riding on the airspring force of the shock struts. A calibration on the main-gear system correlated the effect of skid vertical force F_{v_m} on shock-strut cylinder reaction and shock-strut displacement.

True ground speed during the runout was determined by correlating the velocity obtained from Askania cinetheodolite information with the true ground speed at touchdown calculated from the time-distance relationship between the main-gear and nose-gear impact.

An alternate method for calculating the coefficient of friction of the main-gear skids made use of the following relation to determine the drag-reaction force at the skids

$$F_{h_m} = W_L a_l - D_A$$

The nose-gear drag-reaction force F_{h_n} during the landing run was considered too high in magnitude to be used for rolling resistance. The nose-gear-loads calibration showed the drag due to pure rolling resistance to be unreliable. However, the values of vertical ground reaction were considered satisfactory, and the solution for F_{h_n} was obtained by using vertical reaction and assuming a value of coefficient of friction between the nose-gear wheels and the lakebed. For an analysis of the X-2 airplane (ref. 7), $\mu_n = 0.05$ was used with a satisfactory degree of accuracy. This value appears to compare favorably with an average of calculated results made by using the following relation

$$\mu_n = \frac{W_L a_l - F_{h_m} - D_A}{F_{v_n}}$$

where F_{h_m} is the skid drag force obtained from the drag-brace loads.

The aerodynamic drag D_A was calculated by using the relation

$$D_A = C_D q S$$

where C_D is the airplane drag coefficient corresponding to extended landing gear and full flaps and speed brakes. Flaps were full down before landing and remained down during the runout, and speed brakes were deployed 15 seconds after initial touchdown. Coefficient of friction was calculated for the landing from 15 seconds after touchdown to the end of the runout (corresponding to a true ground speed of 103 knots). The dynamic pressure q was calculated by using data obtained from the sensitive airspeed recording. The results of this analysis are presented in figure 12.

UNCLASSIFIED

REFERENCES

1. Skopinski, T. H., Aiken, William S., Jr., and Huston, Wilber B.: Calibration of Strain-Gage Installations in Aircraft Structures for Measurement of Flight Loads. NACA TN 2993, 1953.

2. Weil, Joseph, and Matranga, Gene J.: Review of Techniques Applicable to the Recovery of Lifting Hypervelocity Vehicles. NASA TM X-334, 1960.

3. McKay, James M.: Measurements Obtained During the First Landing of the North American X-15 Research Airplane. NASA TM X-207, 1959.

4. Flight Research Center: Aerodynamic and Landing Measurements Obtained During the First Powered Flight of the North American X-15 Research Airplane. NASA TM X-269, 1960.

5. Houbolt, John C., and Batterson, Sidney A.: Some Landing Studies Pertinent to Glider-Reentry Vehicles. NASA TN D-448, 1960.

6. Finch, Thomas W., and Matranga, Gene J.: Launch, Low-Speed, and Landing Characteristics Determined From the First Flight of the North American X-15 Research Airplane. NASA TM X-195, 1959.

7. Walker, H., Deutschman, J., and van Summern, J.: Pitch Landing Condition. Nose-Gear Loads. Rep. No. 52-941-010, Bell Aircraft Corp., April 1953. (Rev. July 1954).

TABLE I.- PHYSICAL CHARACTERISTICS OF THE AIRPLANE

Wing:	
Airfoil section	NACA 66005 (Modified)
Total area (includes 94.98 sq ft covered by fuselage), sq ft	200
Span, ft	22.36
Mean aerodynamic chord, ft	10.27
Root chord, ft	14.91
Tip chord, ft	2.98
Taper ratio	0.20
Aspect ratio	2.50
Sweep at 25-percent chord line, deg	25.64
Incidence, deg	0
Dihedral, deg	0
Aerodynamic twist, deg	0
Flap -	
Type	Plain
Area (each), sq ft	8.30
Span (each), ft	4.50
Inboard chord, ft	2.61
Outboard chord, ft	1.08
Deflection, down (nominal design), deg	40
Ratio flap chord to wing chord	0.22
Ratio total flap area to wing area	0.08
Ratio flap span to wing semispan	0.40
Trailing-edge angle, deg	5.67
Sweepback angle of hinge line, deg	0
Horizontal tail:	
Airfoil section	NACA 66005 (Modified)
Total area (includes 63.29 sq ft covered by fuselage), sq ft	115.34
Span, ft	18.08
Mean aerodynamic chord, ft	7.05
Root chord, ft	10.22
Tip chord, ft	2.11
Taper ratio	0.21
Aspect ratio	2.83
Sweep at 25-percent-chord line, deg	45
Dihedral, deg	-15
Ratio horizontal-tail area to wing area	0.58
Movable surface area, sq ft	51.77
Deflection -	
Longitudinal, up, deg	15
Longitudinal, down, deg	35
Lateral differential (pilot authority), deg	±15
Lateral differential (autopilot authority), deg	±30
Control system	Irreversible hydraulic boost with artificial feel
Upper vertical tail:	
Airfoil section	10° single wedge
Total area, sq ft	40.91
Span, ft	4.58
Mean aerodynamic chord, ft	8.95
Root chord, ft	10.21
Tip chord, ft	7.56
Taper ratio	0.74
Aspect ratio	0.51
Sweep at 25-percent-chord line, deg	23.41
Ratio vertical-tail area to wing area	0.20

UNCLASSIFIED

TABLE I.- PHYSICAL CHARACTERISTICS OF THE AIRPLANE - Concluded

Movable surface area, sq ft	26.45
Deflection, deg	±7.50
Sweepback of hinge line, deg	0
Control system	Irreversible hydraulic boost with artificial feel
Lower vertical tail:	
Airfoil section	10° single wedge
Total area, sq ft	34.41
Span, ft	3.83
Mean aerodynamic chord, ft	9.17
Root chord, ft	10.21
Tip chord, ft	8
Taper ratio	0.78
Aspect ratio	0.43
Sweep at 25-percent-chord line, deg	23.41
Ratio vertical-tail area to wing area	0.17
Movable surface area, sq ft	19.95
Deflection, deg	±7.50
Sweepback of hinge line, deg	0
Control system	Irreversible hydraulic boost with artificial feel
Fuselage:	
Length, ft	50.75
Maximum width, ft	7.33
Maximum depth, ft	4.67
Maximum depth over canopy, ft	4.97
Side area (total), sq ft	215.66
Fineness ratio	10.91
Main landing gear:	
Type	Two (6 in. wide, 3 ft long) skids
Shock strut	Oleopneumatic (inside fuselage)

	Original gear	Present gear
Strut-inflation pressure, (fully extended), psi	750	1200
Shock-strut stroke, in.	2.577	3.58
Tread distance (no load), ft	7.03	7.34

Nose landing gear:	
Tire type	VII
Tire size	18 × 4.4
Ply rating	8
Rolling radius, in.	8
Wheels	Dual, corotating
Tire pressure, psi	185
Shock strut	Oleopneumatic
Shock-strut-inflation pressure, psi	184 (fully extended)
Shock-strut stroke, in.	18
Moments of inertia (based on average landing weight, 14,500 lb):	
I_X, slug-ft^2	3,600
I_Y, slug-ft^2	83,500
I_Z, slug-ft^2	85,100
I_{XZ}, slug-ft^2	500

TABLE II.- SUMMARY OF TEST CONDITIONS AND MEASURED FORCES

[X-15 number 1 airplane]

Main-gear touchdown																	
Flight number	Landing weight, lb	Vertical velocity, fps	Time of main-landing-gear impact, sec		Incremental vertical acceleration, g			Maximum shock-strut force, lb		Maximum shock-strut deflection, in.		Maximum main-gear tread, ft	Horizontal-tail load, lb (down)	Shock-strut pressure, psi (a)		Center-of-gravity position, percent mean aerodynamic chord
			Left	Right	Left	Right	Center of gravity	Left	Right	Left	Right			Left	Right	
1-1-5	13,234	2.0	0	----	----	2.7	0.6	----	----	----	----	9.48	----	750	750	17.4
1-2-7	13,988	4.8	0	0.03	0.7	.9	.2	9,579	9,710	1.35	1.40	8.51	1,172	1,200	1,200	18.4
1-3-8	14,564	6.5	0.2	0	1.0	.8	----	26,375	15,667	1.97	1.91	----	1,171	1,200	1,200	----
1-4-9	14,641	5.0	0	----	----	----	----	----	----	----	----	8.83	727	1,200	1,200	----
1-5-10	14,610	4.5	0	----	----	----	----	----	----	----	----	----	669	1,200	1,200	----
1-6-11	14,233	1.0	0	.01	.5	.6	.6	6,203	5,957	.18	.11	7.69	1,156	1,200	1,200	----
1-7-12	14,790	1.0	.20	0	.4	.8	.1	5,866	6,079	.10	.16	7.69	1,230	1,200	1,200	18.4
1-8-13	14,444	4.5	0	.01	.8	1.1	.5	9,368	9,425	1.26	.81	8.71	792	1,200	1,200	----

Nose-gear touchdown																	
Flight number	Nose-gear vertical velocity, fps	Time of nose-gear impact, sec	Incremental vertical acceleration, g				Maximum shock-strut force, lb		Maximum shock-strut deflection, in.			Maximum main-gear tread, ft	Maximum horizontal-tail load, lb (down)	Nose-gear shock-strut pressure, psi	Pitching velocity at nose-gear touchdown, radians/sec (down)	Distance from main-gear to nose-gear touchdown, ft	Runout distance, ft
			Left	Right	Nose	Center of gravity	Left	Right	Left	Right	Nose						
1-1-5	17.4	0.52	----	4.8	7.3	2.4	----	----	----	----	----	10.04	----	184	0.445	187	4,760
1-2-7	11.7	.73	1.6	1.7	9.8	.7	46,800	47,818	3.18	3.10	16.74	10.35	5,523	184	.300	247	6,531
1-3-8	12.6	.39	2.6	3.4	10.4	----	41,736	34,884	2.54	2.88	15.34	10.17	5,012	184	.323	194	7,228
1-4-9	13.7	.73	----	----	----	----	----	----	----	----	----	10.29	4,519	190	.350	266	4,714
1-5-10	15.4	.82	----	----	----	----	----	----	----	----	----	10.20	2,754	182	----	264	4,148
1-6-11	13.2	1.41	1.7	2.6	5.5	1.5	36,883	37,087	2.83	2.46	16.74	10.13	4,504	182	.338	497	4,920
1-7-12	12.6	1.34	1.6	2.3	9.6	1.2	43,339	40,229	3.08	2.89	17.70	10.25	4,765	180	.323	487	5,420
1-8-13	14.3	.96	2.3	2.6	9.9	----	38,613	36,598	2.82	2.65	15.90	10.13	4,643	180	.367	348	5,710

[a]Serviced to ±10 psi.

CONFIDENTIAL

TABLE II.- SUMMARY OF TEST CONDITIONS AND MEASURED FORCES - Concluded

[X-15 number 2 airplane]

Main-gear touchdown																
Flight number	Landing weight, lb	Vertical velocity, fps	Time of main-landing-gear impact, sec		Incremental vertical acceleration, g			Maximum shock-strut force, lb		Maximum shock-strut deflection, in.		Maximum main-gear tread, ft	Horizontal-tail load, lb (down)	Shock-strut pressure, psi (a)		Center-of-gravity position, percent mean aerodynamic chord
			Left	Right	Left	Right	Center of gravity	Left	Right	Left	Right			Left	Right	
[b]2-1-3	13,984	5.0 4.2	0	0.06	0.6 1.3	-------	0.3	8,985 18,837	4,607 13,320	0.43 .67	0.35 .64	7.40	1,097	925	925	----------
2-2-6	14,165	7.7	0	.03	1.9	-------	.8	21,500	19,500	.59	.62	7.85	959	1,160	1,140	----------
2-3-9	15,183	9.5	0	.005	2.6	-------	1.4	26,300	26,700	1.68	1.58	8.79	1,664	1,200	1,200	17.3
2-4-11	15,062	6.5	0	.03	1.8	2.2	.8	27,605	28,634	1.89	2.07	9.42	1,639	1,200	1,200	19.3
2-5-12	14,798	3.6	0	.14	.9	.5	.2	6,999	6,324	1.04	.66	8.23	976	1,200	1,200	----------
2-6-13	14,619	2.5	0	.16	.3	.3	.2	6,960	7,139	.94	1.04	7.88	1,102	1,200	1,200	19.1
2-7-15	14,394	2.5	0	.08	.8	.3	----------	5,122	5,975	.10	.15	7.79	1,132	1,200	1,200	19.4
2-8-16	14,583	3.5	0	.07	1.3	.5	.4	8,133	7,566	1.12	.44	8.11	1,399	1,200	1,200	19.3
2-9-18	14,469	4.0	0	.05	.6	.6	----------	6,960	6,440	.83	.52	8.09	----------	1,200	1,200	18.9

Nose-gear touchdown																			
Flight number	Nose-gear vertical velocity, fps	Time of nose-gear impact, sec	Incremental vertical acceleration, g				Maximum shock-strut force, lb		Maximum shock-strut deflection, in.			Maximum main-gear tread, ft	Maximum horizontal-tail load, lb (down)	Nose-gear shock-strut pressure, psi	Pitching velocity at nose-gear touchdown, radians/sec (down)	Maximum nose-gear reaction, lb		Distance from main-gear to nose-gear touchdown, ft	Runout distance, ft
			Left	Right	Nose	Center of gravity	Left	Right	Left	Right	Nose					Vertical	Spin-up drag (c)		
2-1-3	13.2	0.85	1.7	-------	-------	1.3	35,071	37,407	2.75	2.58	-------	9.50	6,434	184	0.337	-------	-------	330	5,560
2-2-6	12.1	.51	3.5	-------	-------	3.0	34,500	35,750	2.42	2.34	18.00	9.38	4,638	184	.309	-------	-------	203	4,252
2-3-9	16.5	.59	2.2	-------	6.3	4.3	35,200	34,500	2.59	2.41	18.00	9.21	5,448	184	.422	-------	-------	184	1,561
2-4-11	12.3	.46	2.4	2.8	7.3	1.6	40,664	43,301	2.90	3.20	17.29	10.25	4,758	175	.315	15,854	9,870	184	5,734
2-5-12	12.6	.95	4.1	4.0	9.1	1.7	40,400	40,400	2.98	2.93	15.83	10.23	5,039	330	.323	19,789	10,580	332	4,669
2-6-13	7.8	.93	1.9	1.7	6.8	1.3	37,106	35,580	2.77	2.67	16.46	9.96	5,308	178	.200	14,029	8,430	355	6,073
2-7-15	12.6	.98	2.4	2.3	10.5	----------	36,324	37,908	2.73	2.74	16.31	10.10	5,632	184	.323	15,708	12,900	357	5,938
2-8-16	7.6	.80	2.6	1.6	9.2	1.9	44,457	46,482	3.26	3.04	17.41	10.36	5,134	184	.195	16,764	15,040	297	5,625
2-9-18	16.0	1.10	2.3	2.1	13.1	----------	37,106	36,278	2.77	2.87	17.65	10.14	----------	184	.410	25,394	-------	339	4,330

[a]Serviced to ±10 psi.
[b]Initial contact followed by rebound.
[c]Incremental drag force.

CONFIDENTIAL

TABLE III.- PRETOUCHDOWN CONDITIONS

Flight number	Pilot	Landing weight, lb	Wind conditions		Velocity at touchdown, KIAS	Vertical velocity, fps	True ground speed at touchdown, knots	Runway		Indicated angle of attack, deg	Pitch velocity, radians/sec	Roll velocity, radians/sec	Sideslip angle, deg	Flap angle, deg	Center-of-gravity acceleration, g
			Velocity, knots	Direction				Magnetic heading	Condition						
[X-15 number 1]															
1-1-5	A	13,234	[a] Calm	----------	153	2.0	168	350	Dry, hard	8.5	0.024 (down)	0.091 (right)	0.7 (left)	38.0	1.40
1-2-7	A	13,988	Calm	West	189	4.8	168	180	Damp, hard	7.1	.004 (down)	.012 (right)	.7 (right)	38.0	1.20
1-3-8	B	14,564	21	Southwest	214	6.5	238	350	Dry, hard	4.7	.025 (down)	.025 (left)	1.6 (left)	41.9	1.20
1-4-9	C	14,641	Calm	----------	174	5.0	184	350	Dry, hard	7.6	1.250 (up)	.005 (left)	.1 (right)	42.3	----------
1-5-10	B	14,610	18	Southwest	180	4.5	163	250	Dry, hard	7.5	----------	----------	----------	42.5	----------
1-6-11	C	14,233	Calm	North	189	1.0	192	350	Dry, hard	7.4	.019 (up)	.060 (right)	.2 (left)	28.5	1.10
1-7-12	B	14,790	23	West-southwest	193	1.0	198	180	Dry, hard	5.2	.018 (down)	.066 (right)	.94 (right)	28.7	.95
1-8-13	C	14,444	19	North-northeast	173	4.5	190	180	Dry, hard	7.7	.048 (up)	.019 (left)	.32 (left)	29.6	1.0
[X-15 number 2]															
2-1-3	A	13,984	9	Southwest	184	5.0 4.2	203	350	Dry, hard	8.1	0.045 (up)	0.013 (right)	0.88 (left)	23.2	1.15
2-2-6	A	14,165	Calm	Northwest	180	7.7	191	350	Dry, hard	7.6	.047 (down)	.020 (right)	.49 (left)	37.6	1.08
2-3-9	A	15,183	18	Northwest	161	9.5	145	Rosamond Dry Lake	Dry, hard	10.8	.036 (up)	.008 (left)	3.2 (left)	37.2	.85
2-4-11	A	15,062	4	Southwest	188	6.5	185	350	Dry, hard	6.2	.008 (up)	.056 (left)	1.2 (left)	33.8	1.00
2-5-12	A	14,798	Calm	----------	185	3.6	183	180	Dry, hard	8.7	.006 (up)	.020 (left)	.44 (left)	32.3	1.25
2-6-13	A	14,619	9	North-northeast	192	2.5	201	180	Dry, hard	6.3	.003 (down)	.032 (right)	1.5 (left)	33.8	1.25
2-7-15	A	14,394	Calm	North-northeast	193	2.5	193	180	Dry, hard	7.1	.013 (up)	.048 (right)	.1 (right)	31.5	1.05
2-8-16	A	14,583	Calm	----------	185	3.5	198	180	Dry, hard	6.6	.021 (up)	.012 (left)	.15 (right)	27.2	.95
2-9-18	A	14,469	Calm	Southeast	160	4.0	161	180	Dry, hard	11.2	.016 (down)	.005 (right)	.50 (right)	26.5	1.10

[a] "Calm" denotes variable from 0 to 3 knots.

UNCLASSIFIED

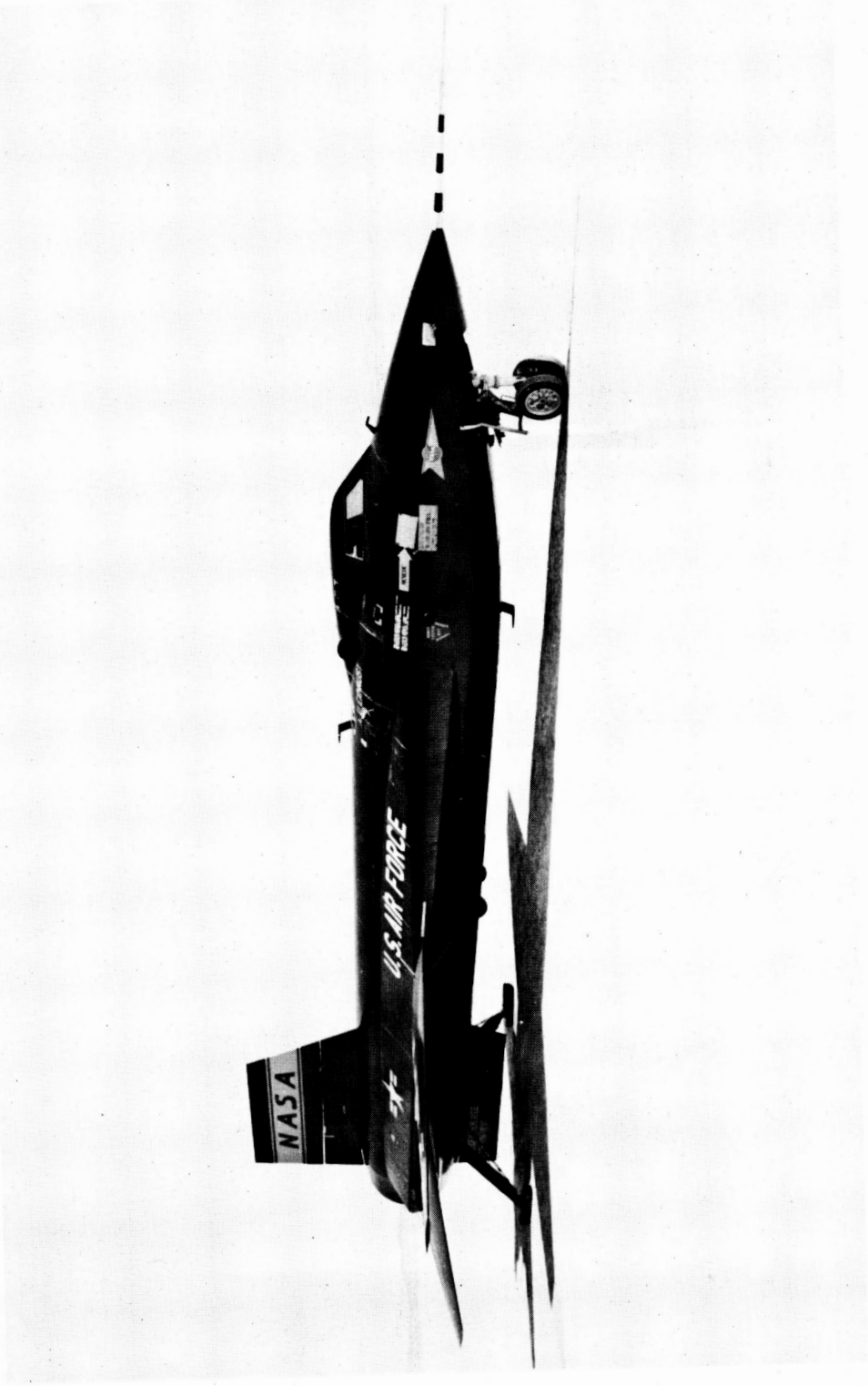

E-5258

Figure 1.- X-15 research airplane.

UNCLASSIFIED

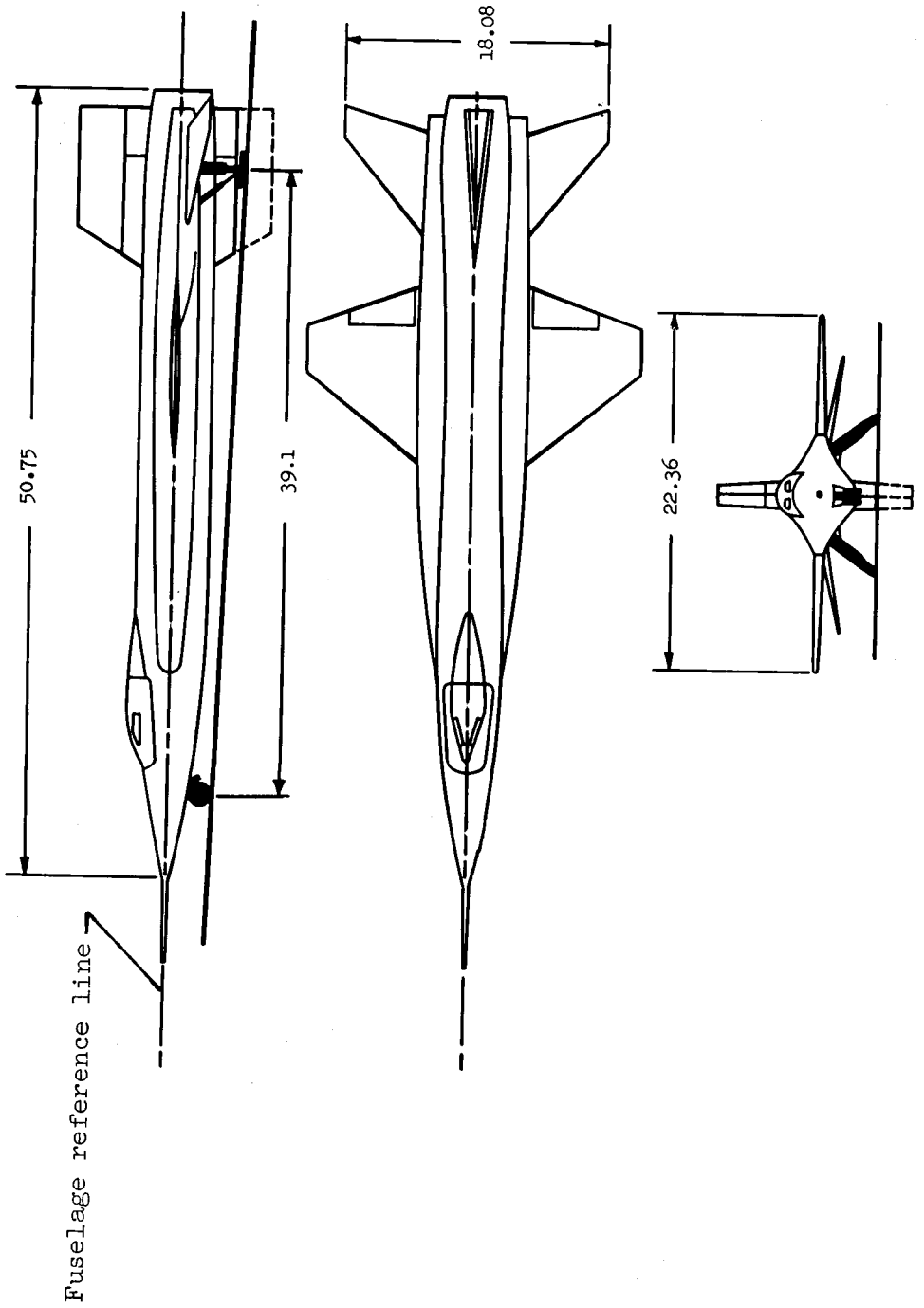

Figure 2.- Three-view drawing of the X-15 airplane. All dimensions in feet.

CONFIDENTIAL

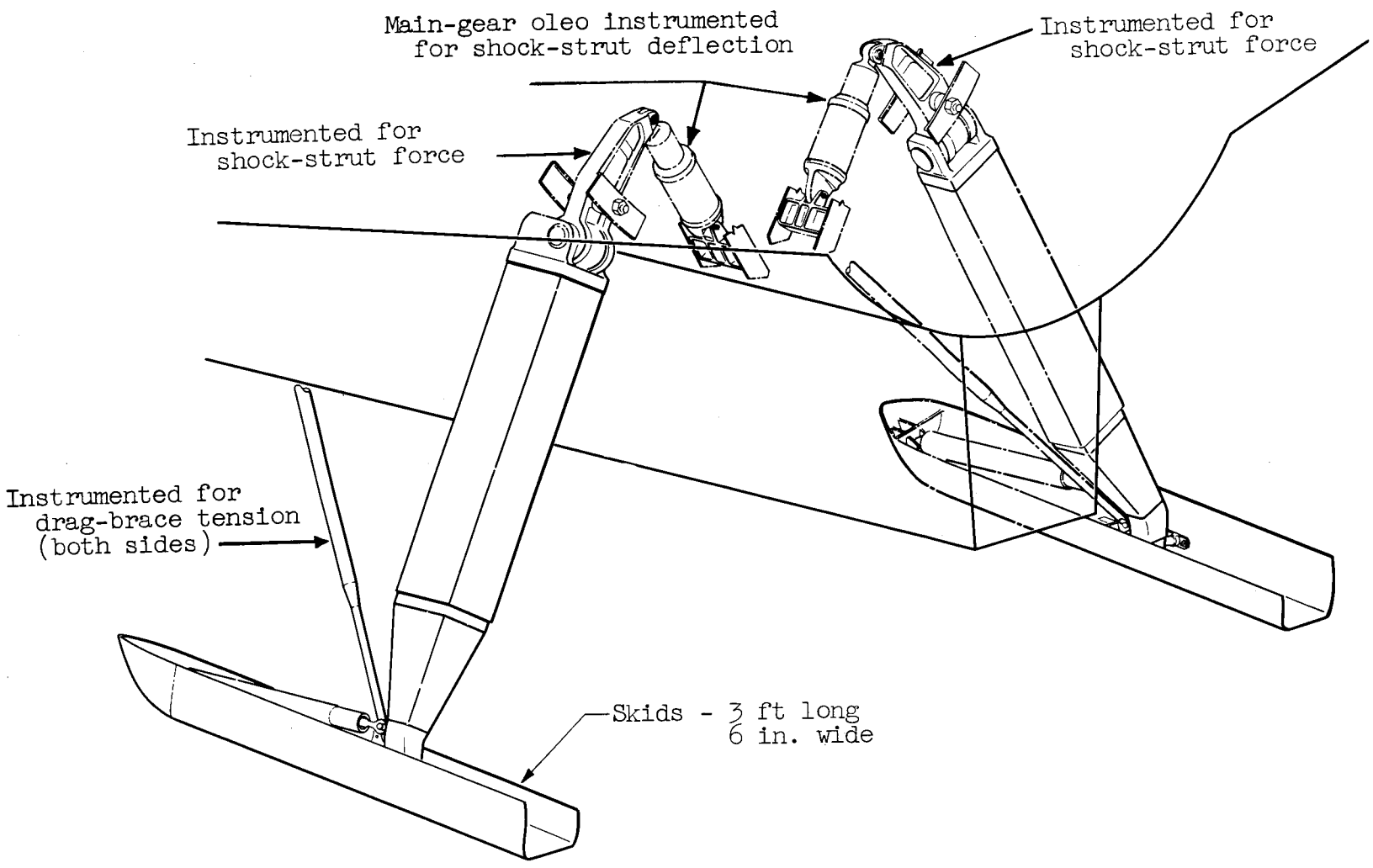

(a) Schematic drawing.

Figure 3.- X-15 main landing gear.

CONFIDENTIAL

UNCLASSIFIED

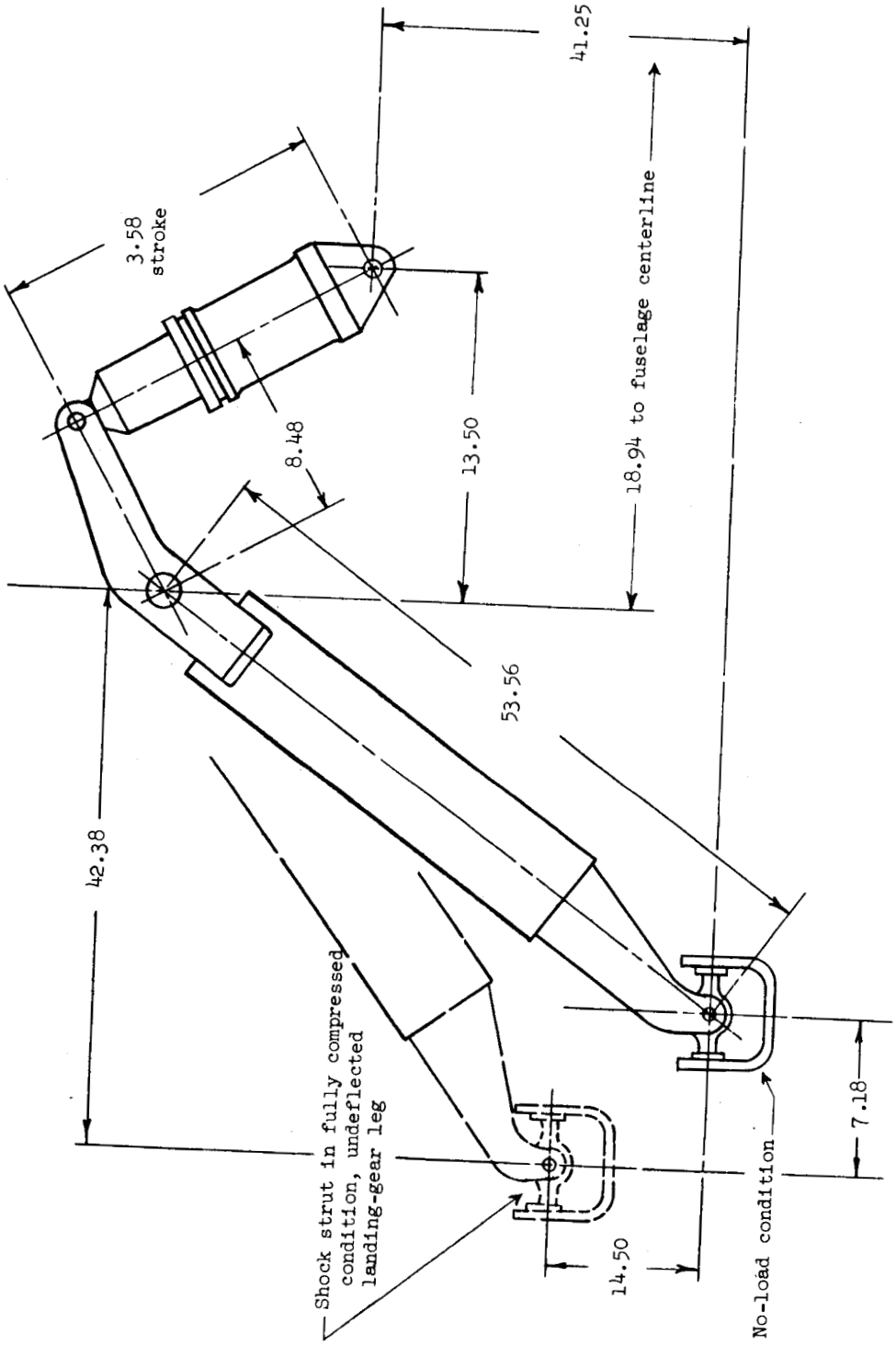

(b) Sketch showing main-gear dimensions in inches. (Not drawn to scale.)

Figure 3.- Concluded.

UNCLASSIFIED

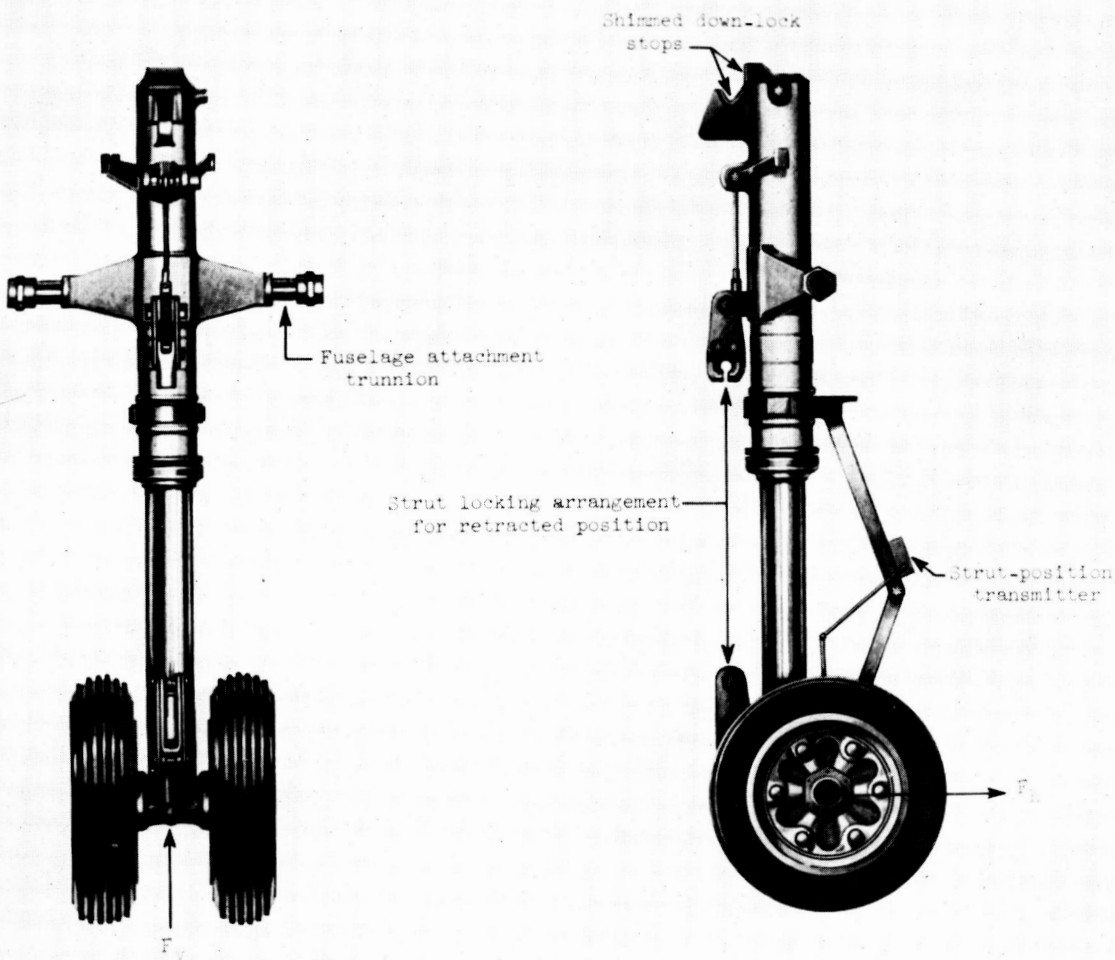

Figure 4.- X-15 nose gear-extended position.

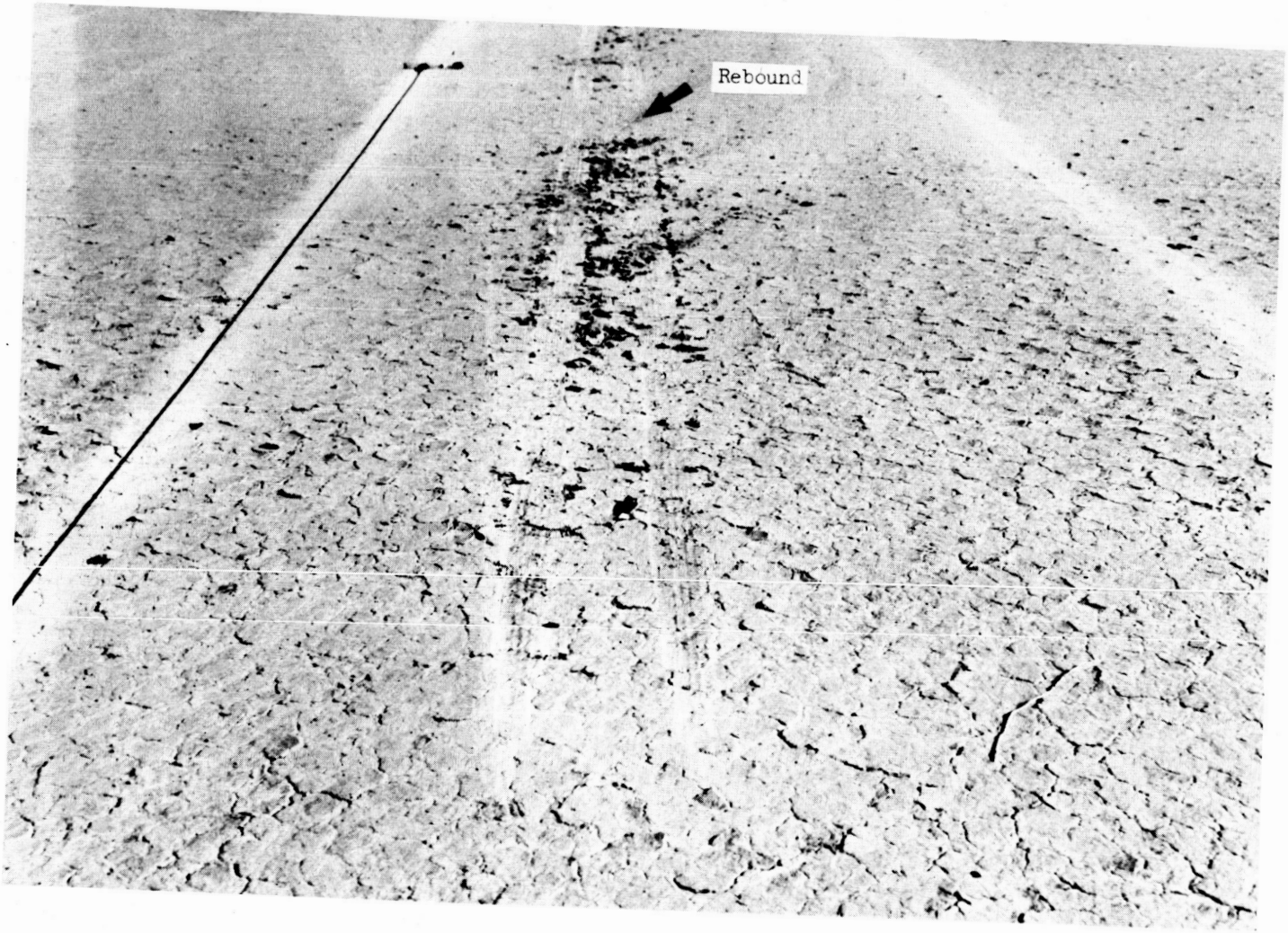

Figure 5.- Typical marks on the lakebed showing rebound due to foaming in the nose-gear shock strut during initial landings of the X-15 airplane.

E-5856

UNCLASSIFIED

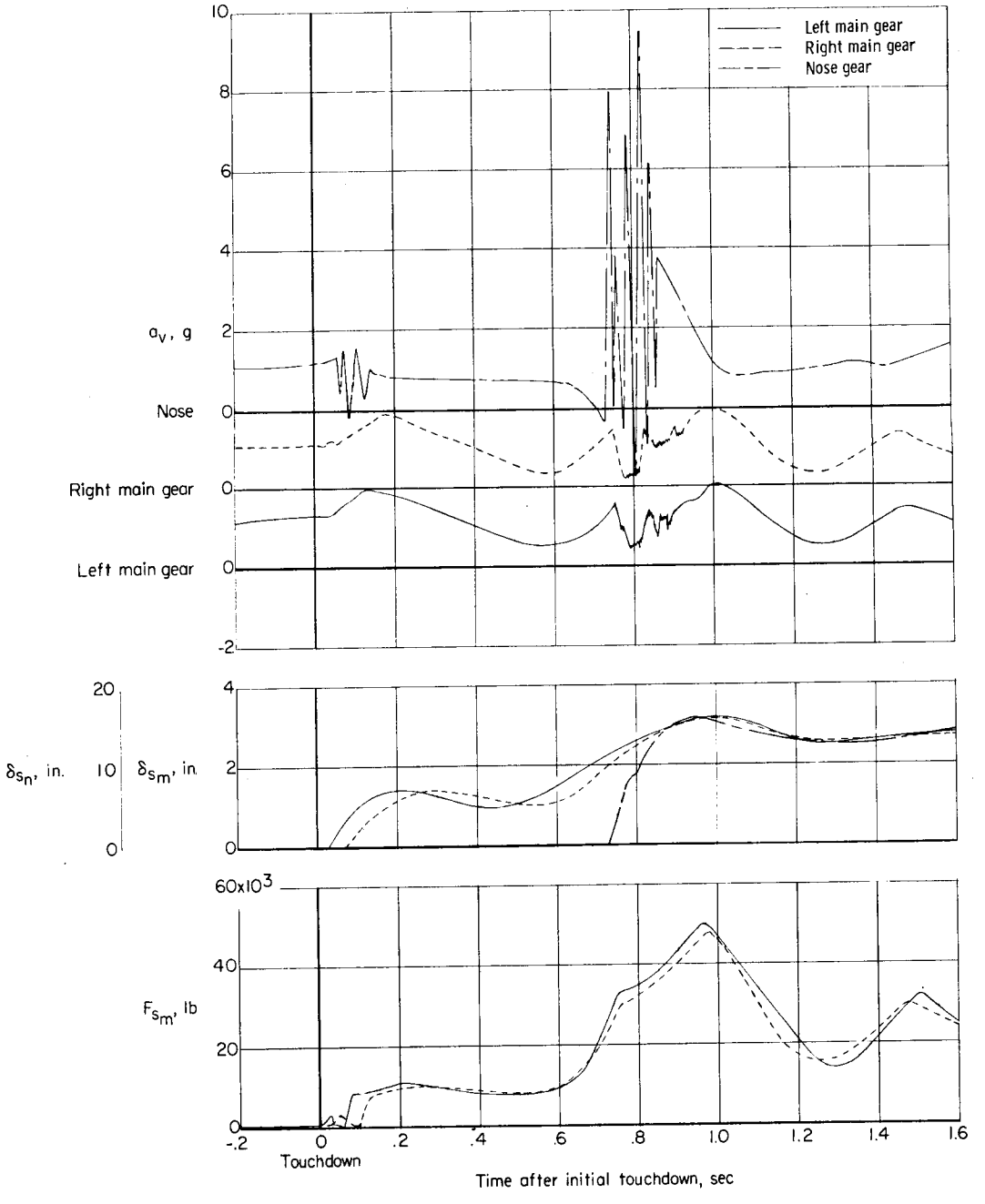

(a) Nose-gear touchdown occurs at $\Delta t_n = 0.730$ second (flight 1-2-7).

Figure 6.- Variation with time of shock-strut force, shock-strut displacement, and upper-mass acceleration during some landings of the X-15 number 1 airplane.

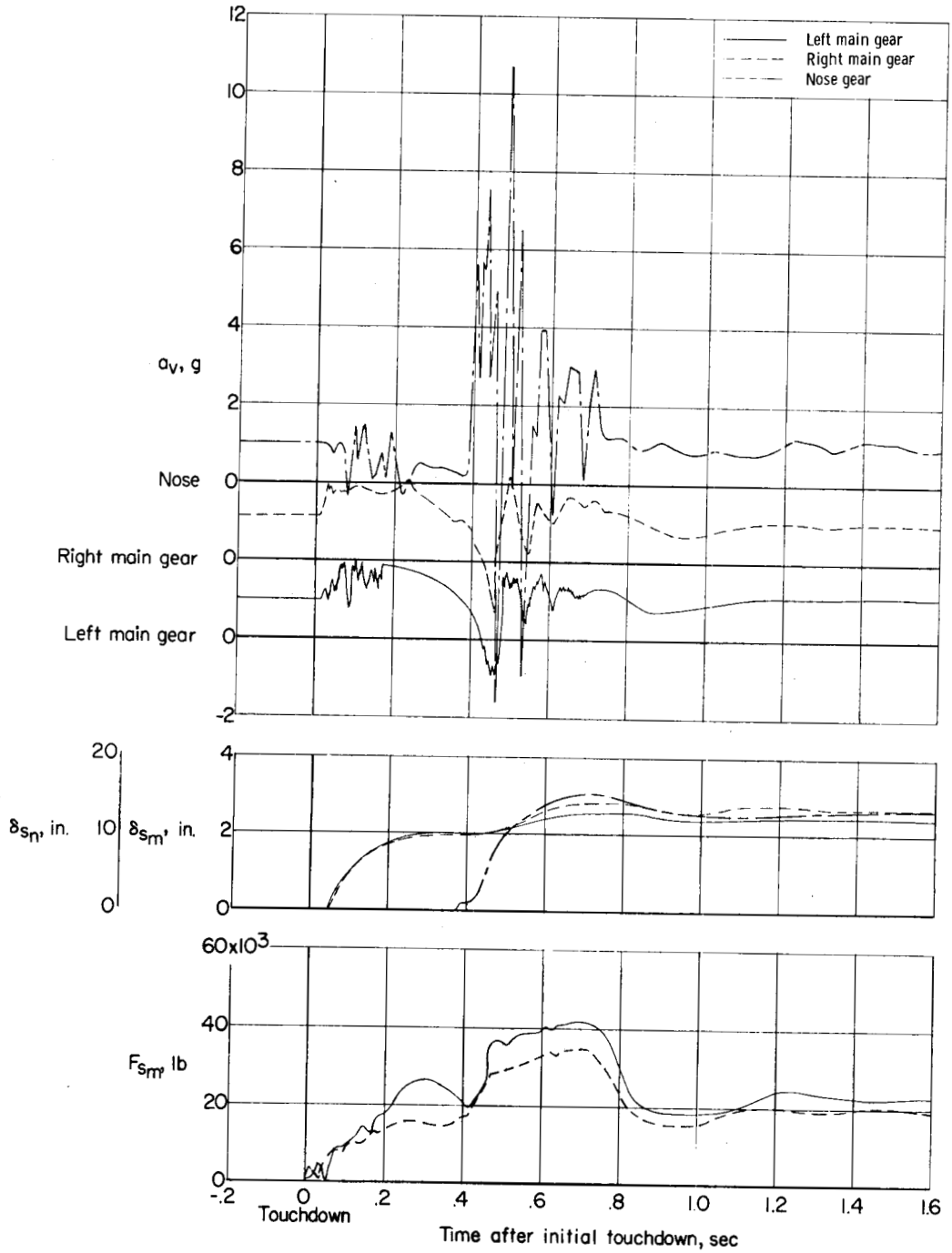

(b) Nose-gear touchdown occurs at $\Delta t_n = 0.385$ second (flight 1-3-8).

Figure 6.- Continued.

UNCLASSIFIED

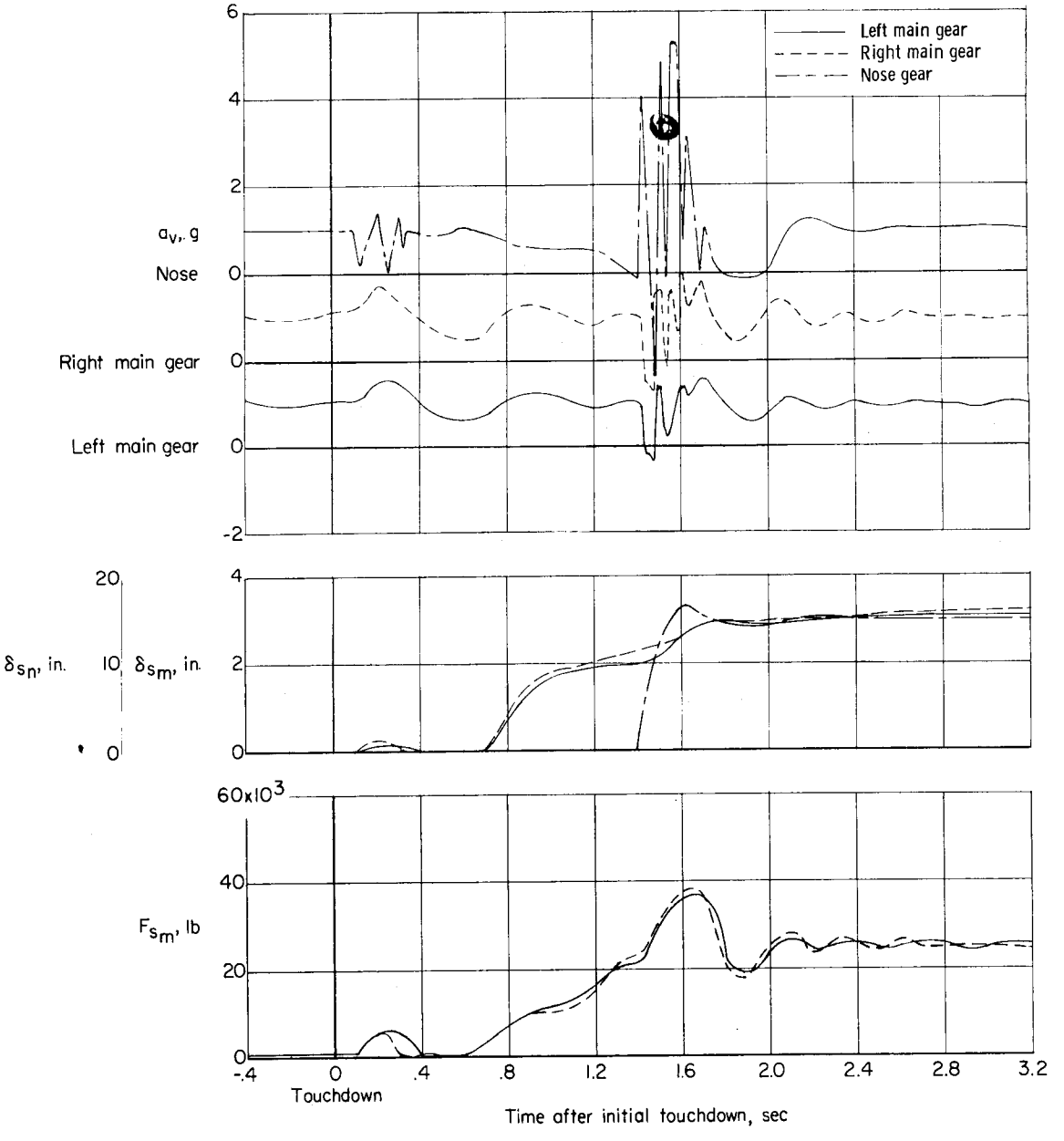

(c) Nose-gear touchdown occurs at Δt_n = 1.410 seconds (flight 1-6-11).

Figure 6.- Continued.

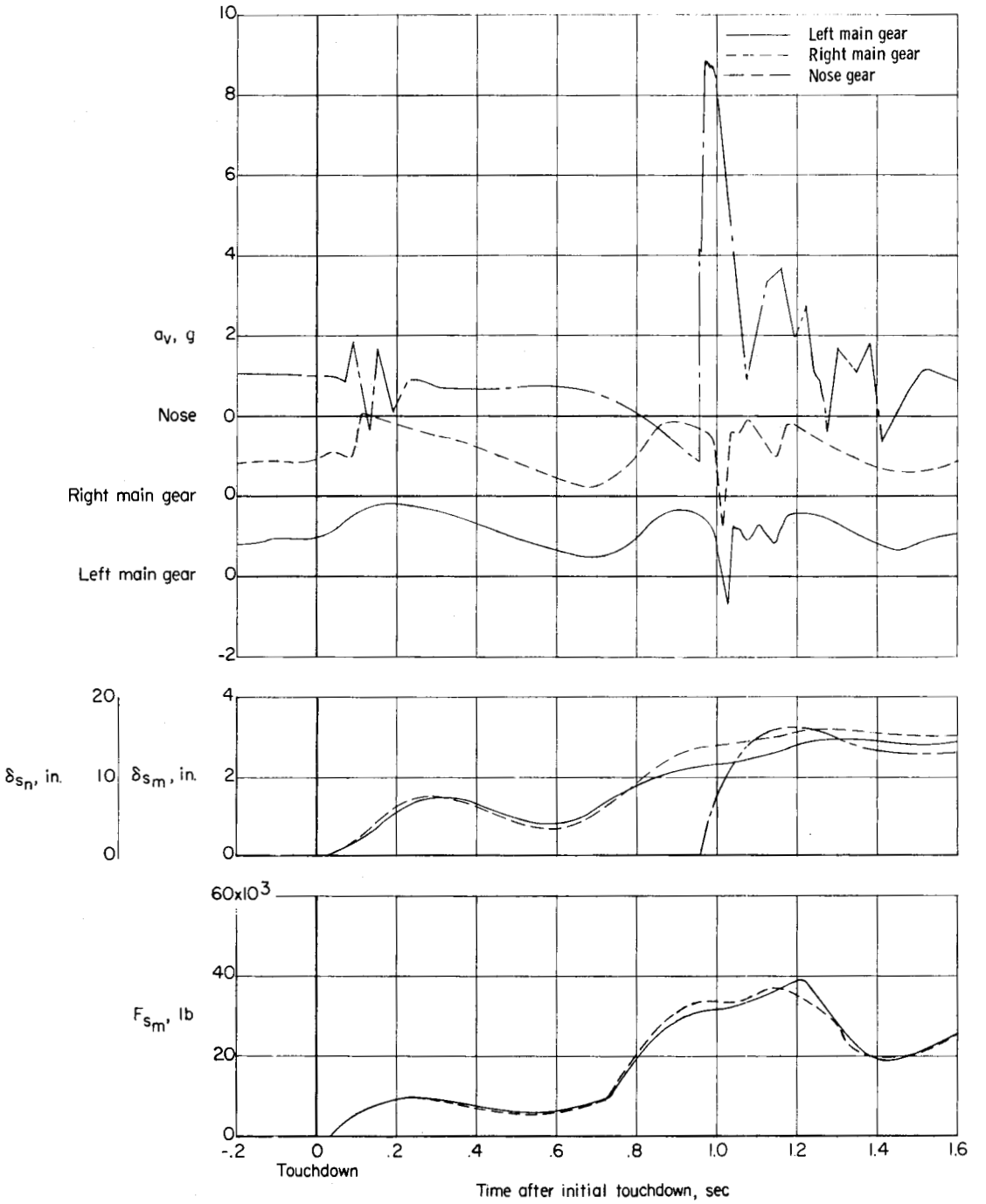

(d) Nose-gear touchdown occurs at $\Delta t_n = 0.960$ second (flight 1-8-13).

Figure 6.- Concluded.

UNCLASSIFIED

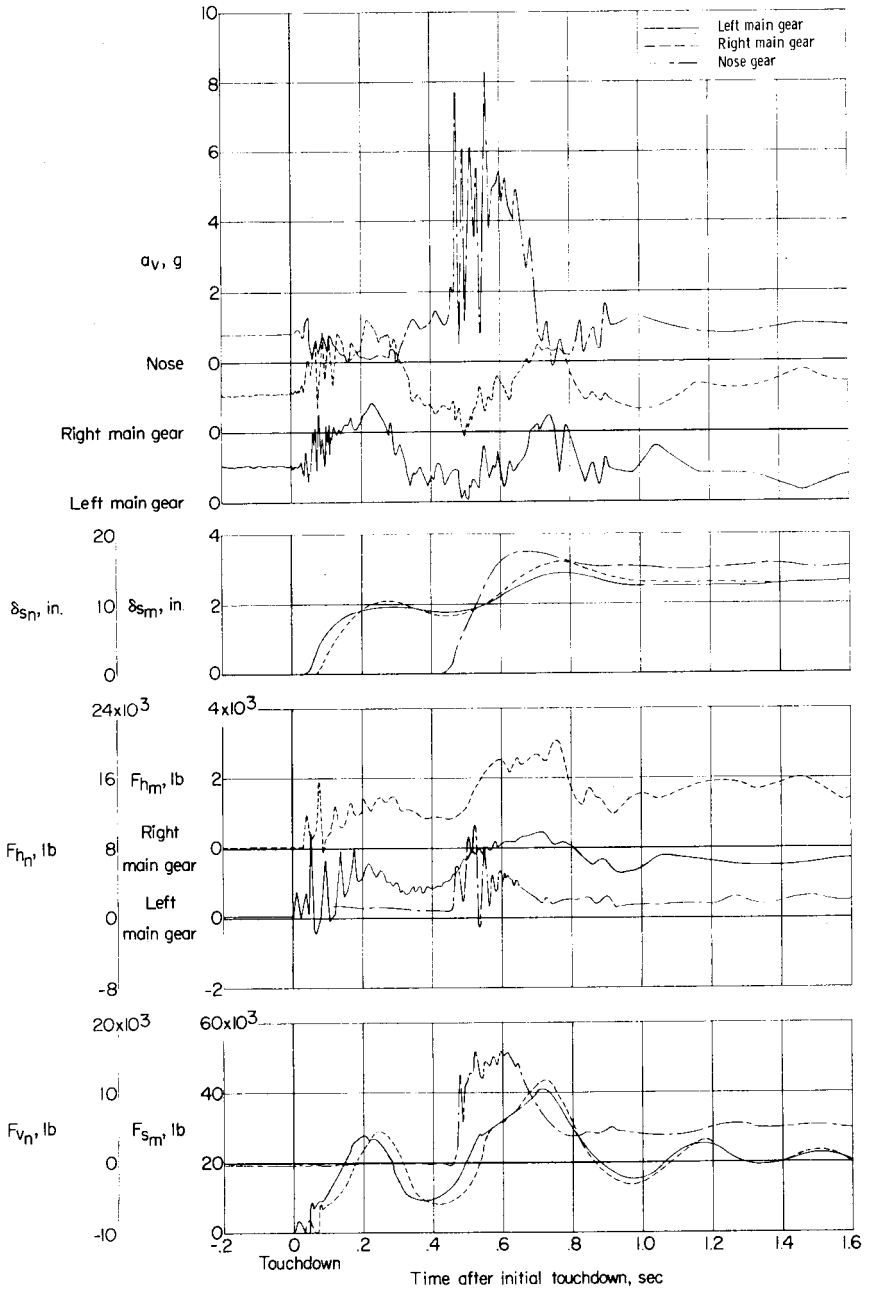

(a) Nose-gear touchdown occurs at $\Delta t_n = 0.455$ second (flight 2-4-11).

Figure 7.- Variation with time of shock-strut force, nose-gear vertical ground reaction, drag ground reaction, shock-strut displacement, and upper-mass acceleration during some landings of the X-15 number 2 airplane.

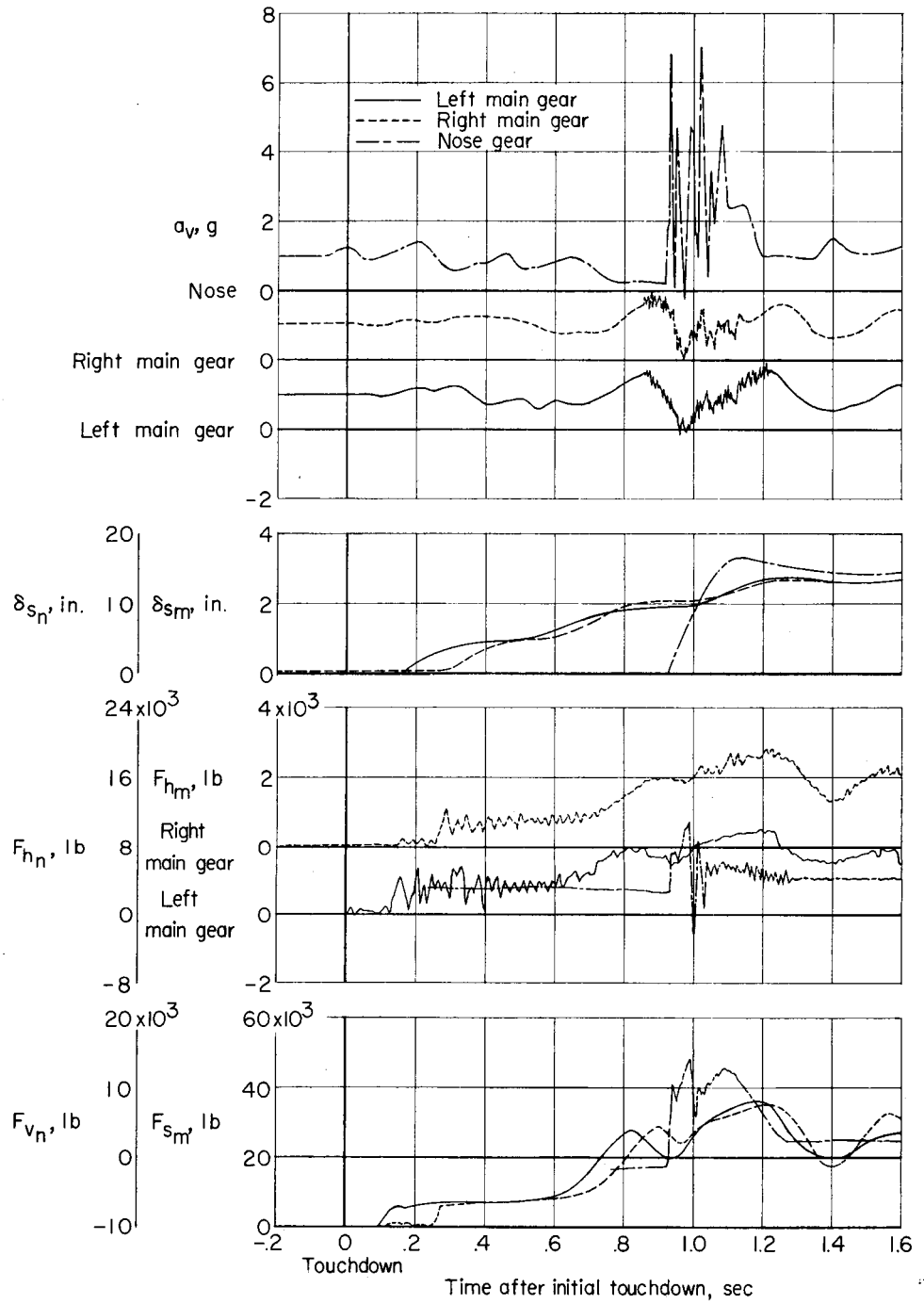

(b) Nose-gear touchdown occurs at $\Delta t_n = 0.928$ second (flight 2-6-13).

Figure 7.- Continued.

UNCLASSIFIED

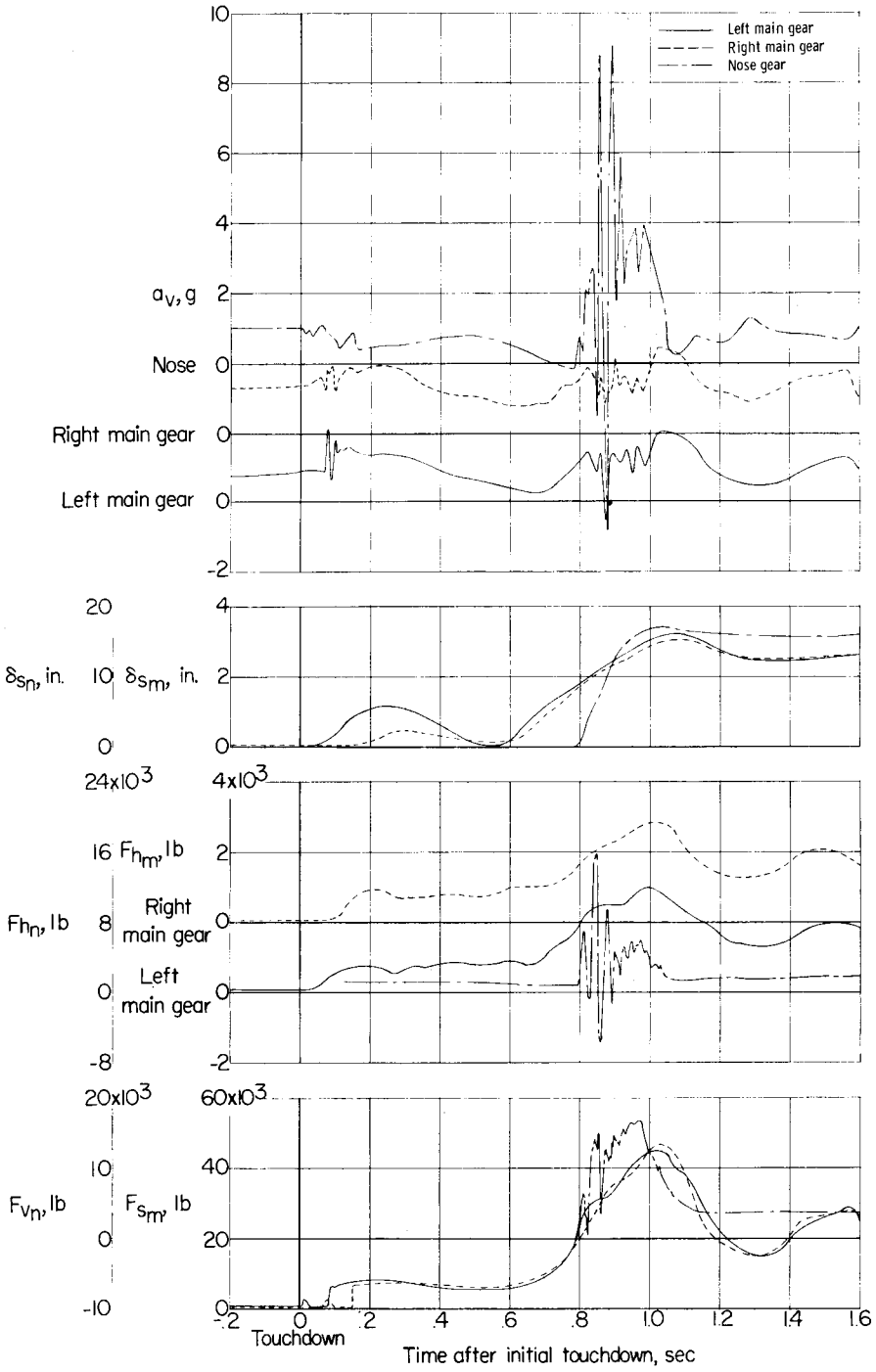

(c) Nose-gear touchdown occurs at $\Delta t_n = 0.795$ second (flight 2-8-16).

Figure 7.- Continued.

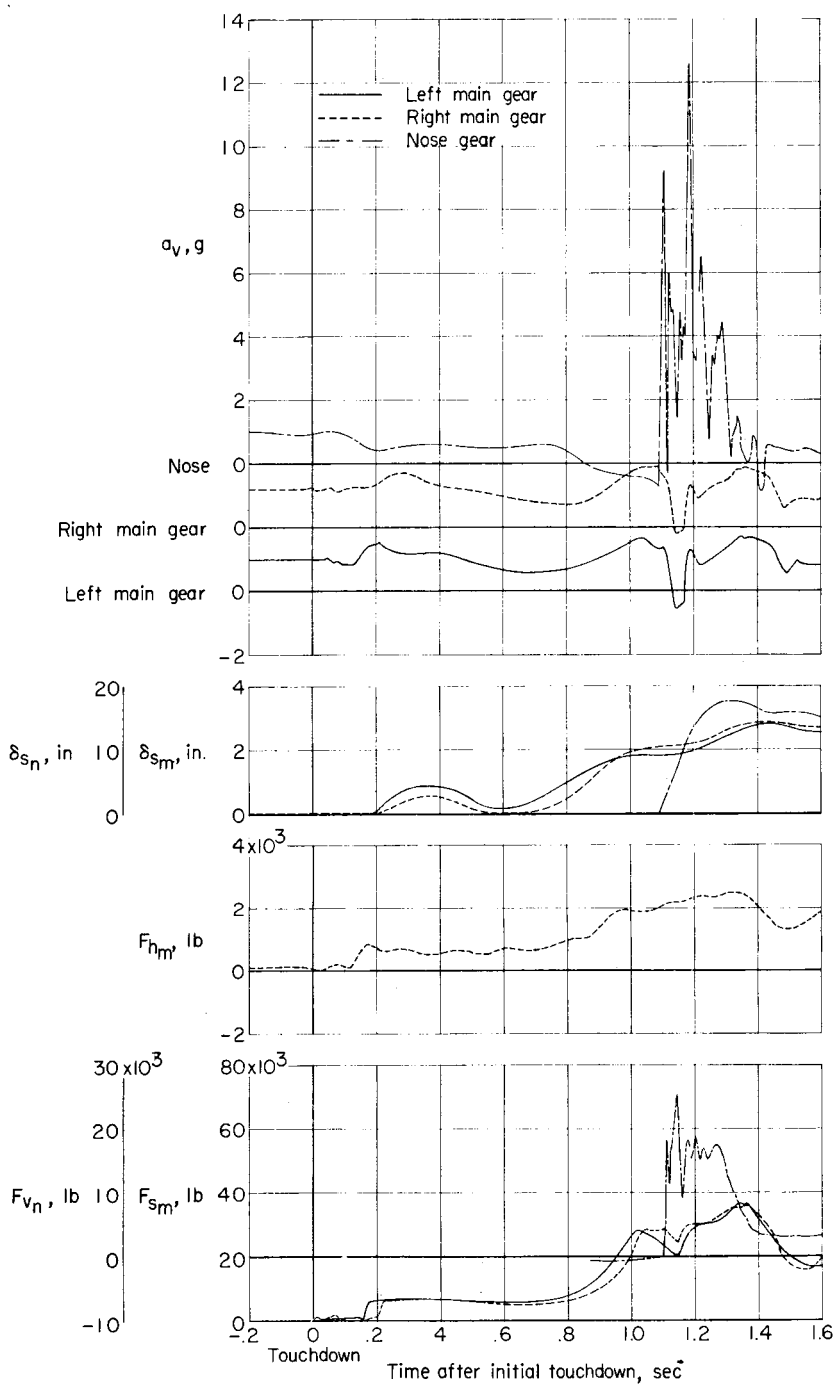

(d) Nose-gear touchdown occurs at $\Delta t_n = 1.090$ seconds (flight 2-9-18).

Figure 7.- Concluded.

UNCLASSIFIED

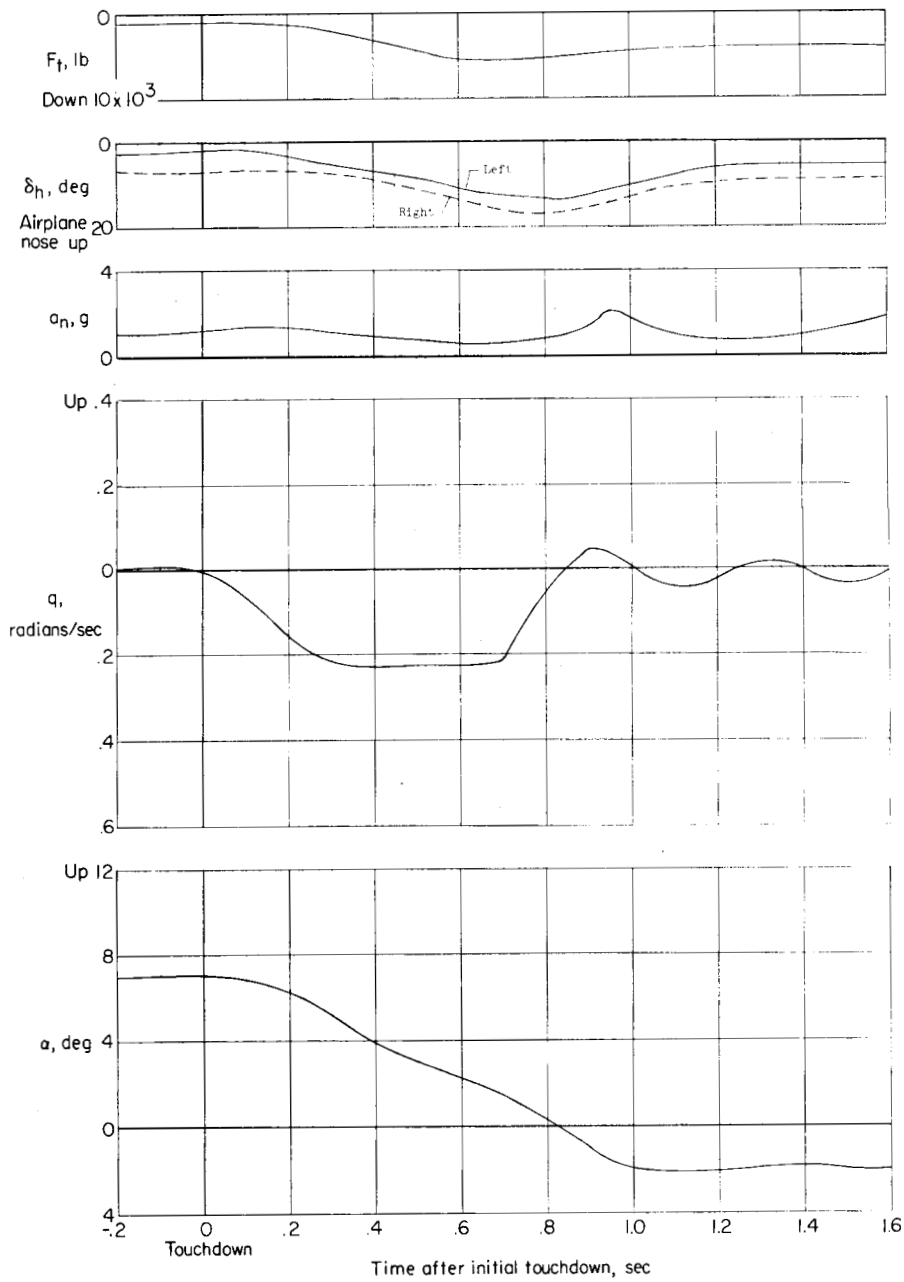

(a) Nose-gear touchdown occurs at $\Delta t_n = 0.730$ second (flight 1-2-7).

Figure 8.- Variation with time of angle of attack, pitching velocity, center-of-gravity vertical acceleration, horizontal-tail deflection, and horizontal-tail load during some landings of the X-15 number 1 airplane.

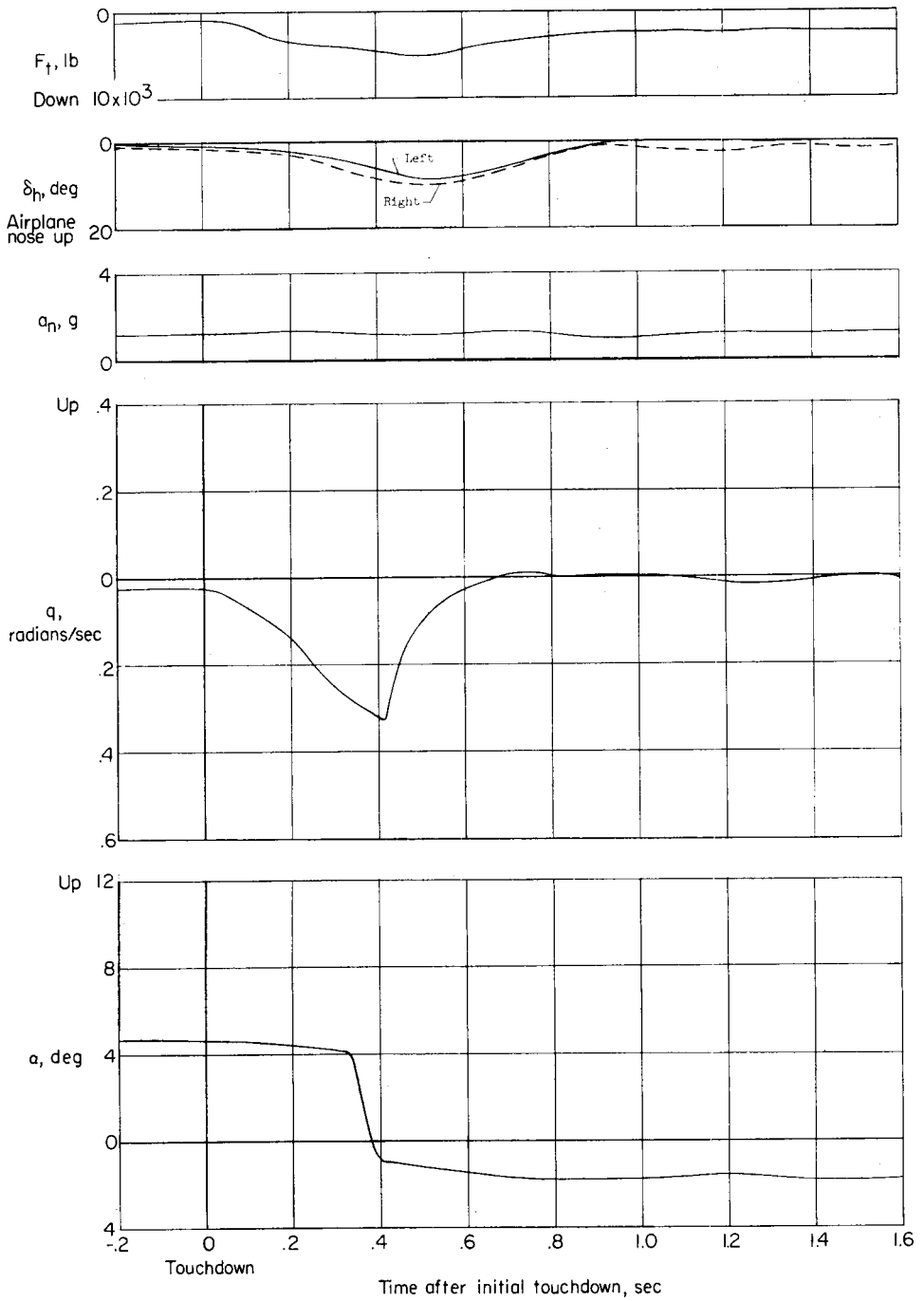

(b) Nose-gear touchdown occurs at $\Delta t_n = 0.385$ second (flight 1-3-8).

Figure 8.- Continued.

UNCLASSIFIED

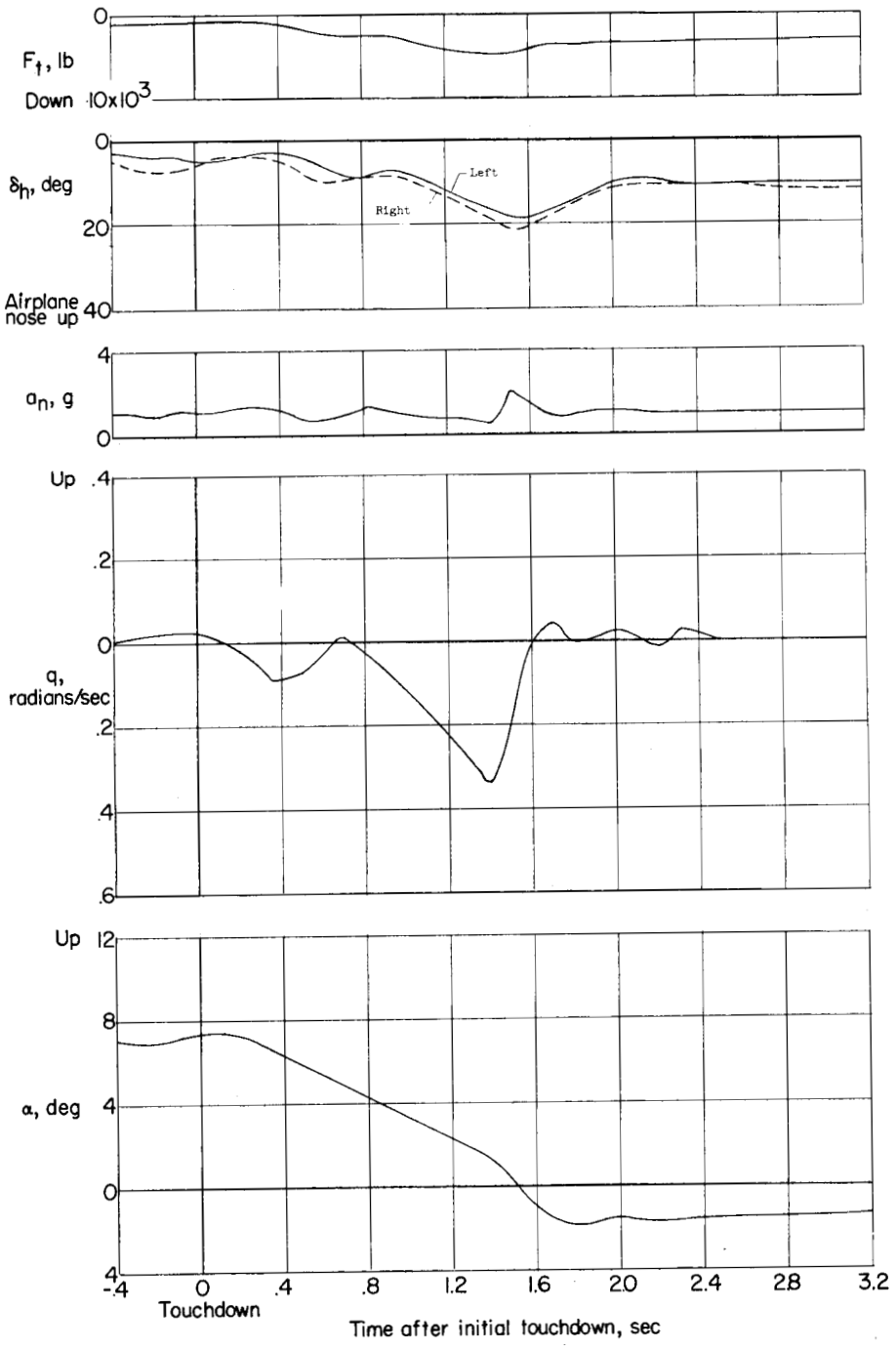

(c) Nose-gear touchdown occurs at Δt_n = 1.410 seconds (flight 1-6-11).

Figure 8.- Continued.

UNCLASSIFIED

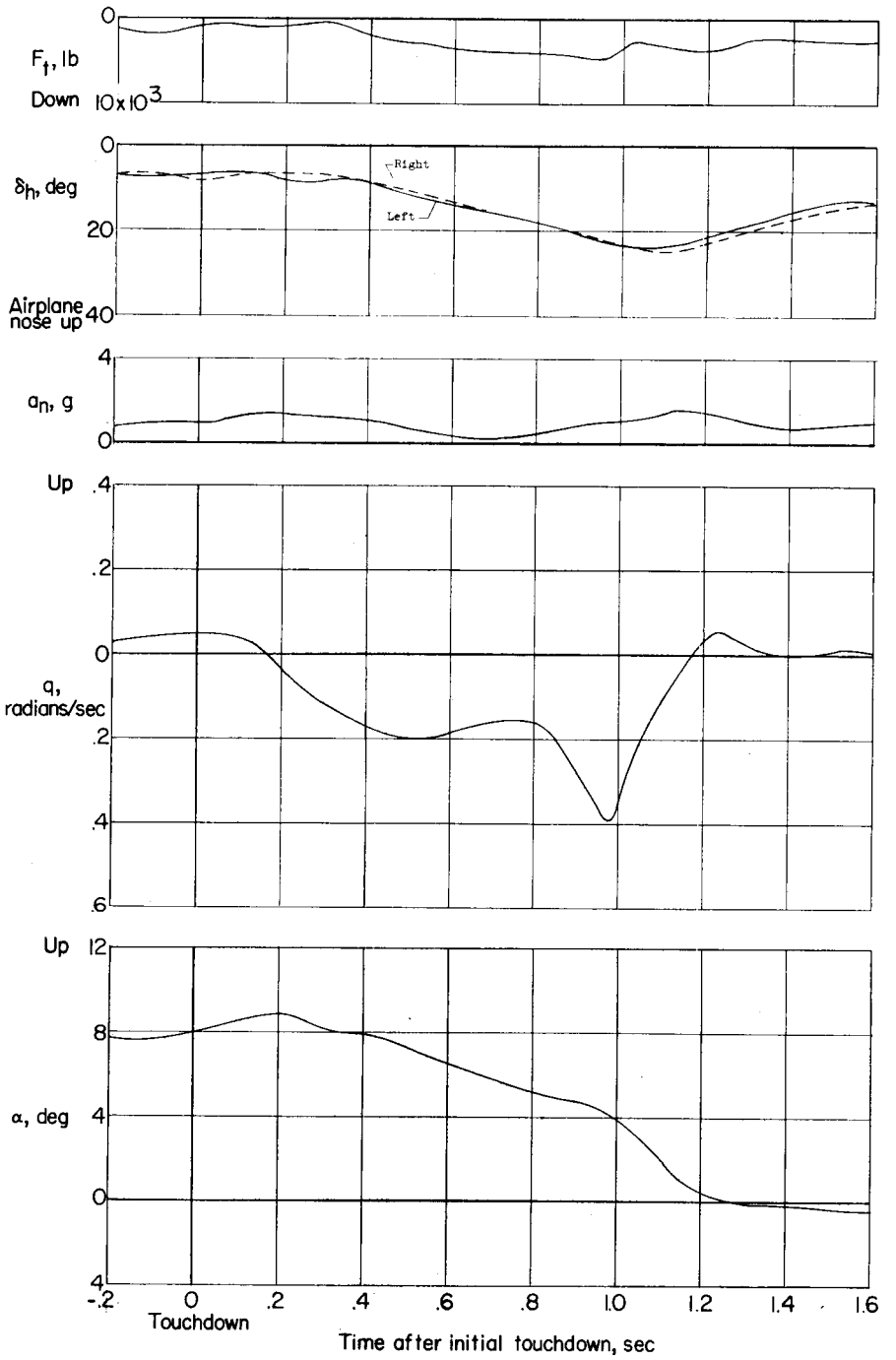

(d) Nose-gear touchdown occurs at $\Delta t_n = 0.960$ second (flight 1-8-13).

Figure 8.- Concluded.

UNCLASSIFIED

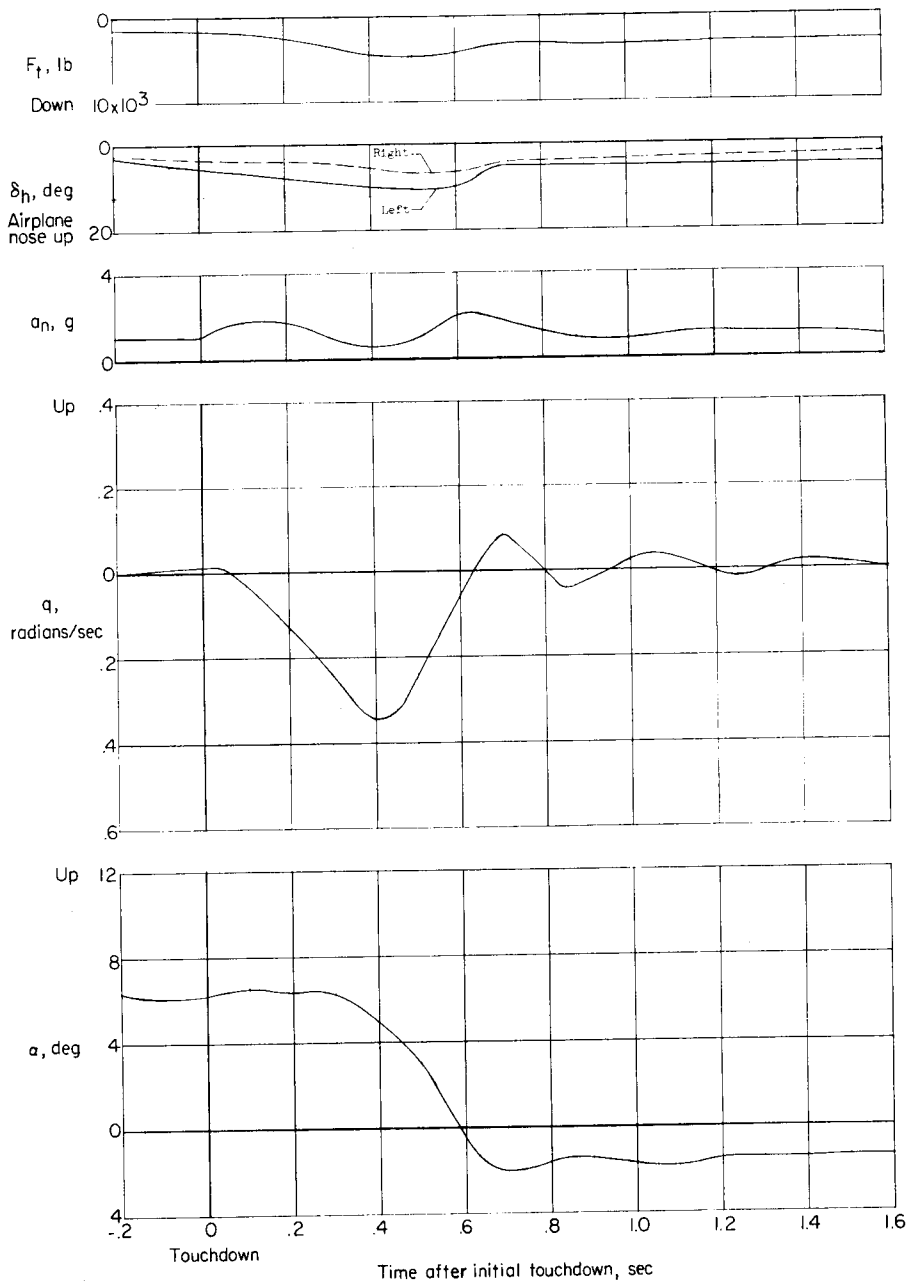

(a) Nose-gear touchdown occurs at $\Delta t_n = 0.455$ second (flight 2-4-11).

Figure 9.- Variation with time of angle of attack, pitching velocity, center-of-gravity vertical acceleration, horizontal-tail deflection, and horizontal-tail load during some landings of the X-15 number 2 airplane.

UNCLASSIFIED

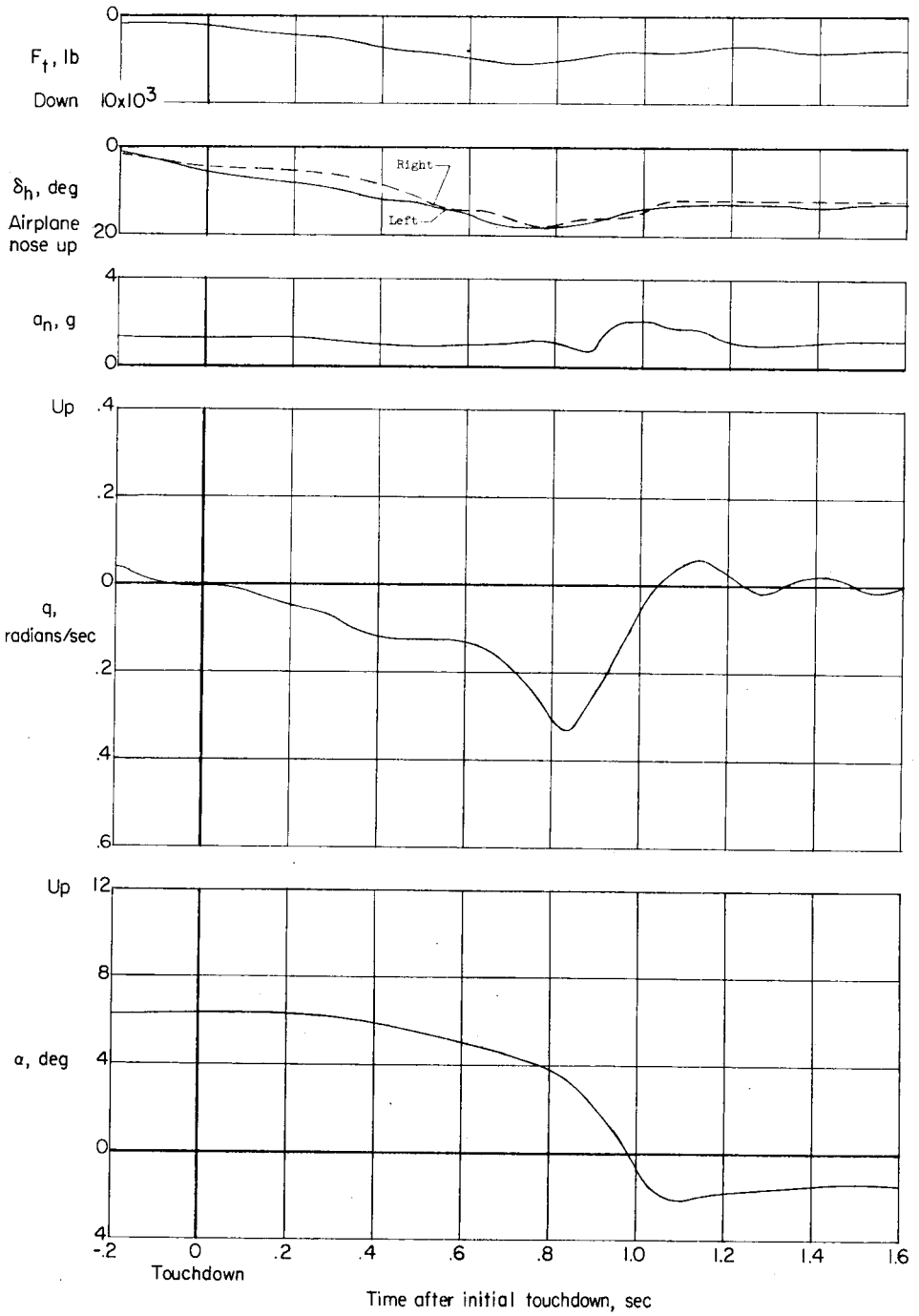

(b) Nose-gear touchdown occurs at $\Delta t_n = 0.928$ second (flight 2-6-13).

Figure 9.- Continued.

UNCLASSIFIED

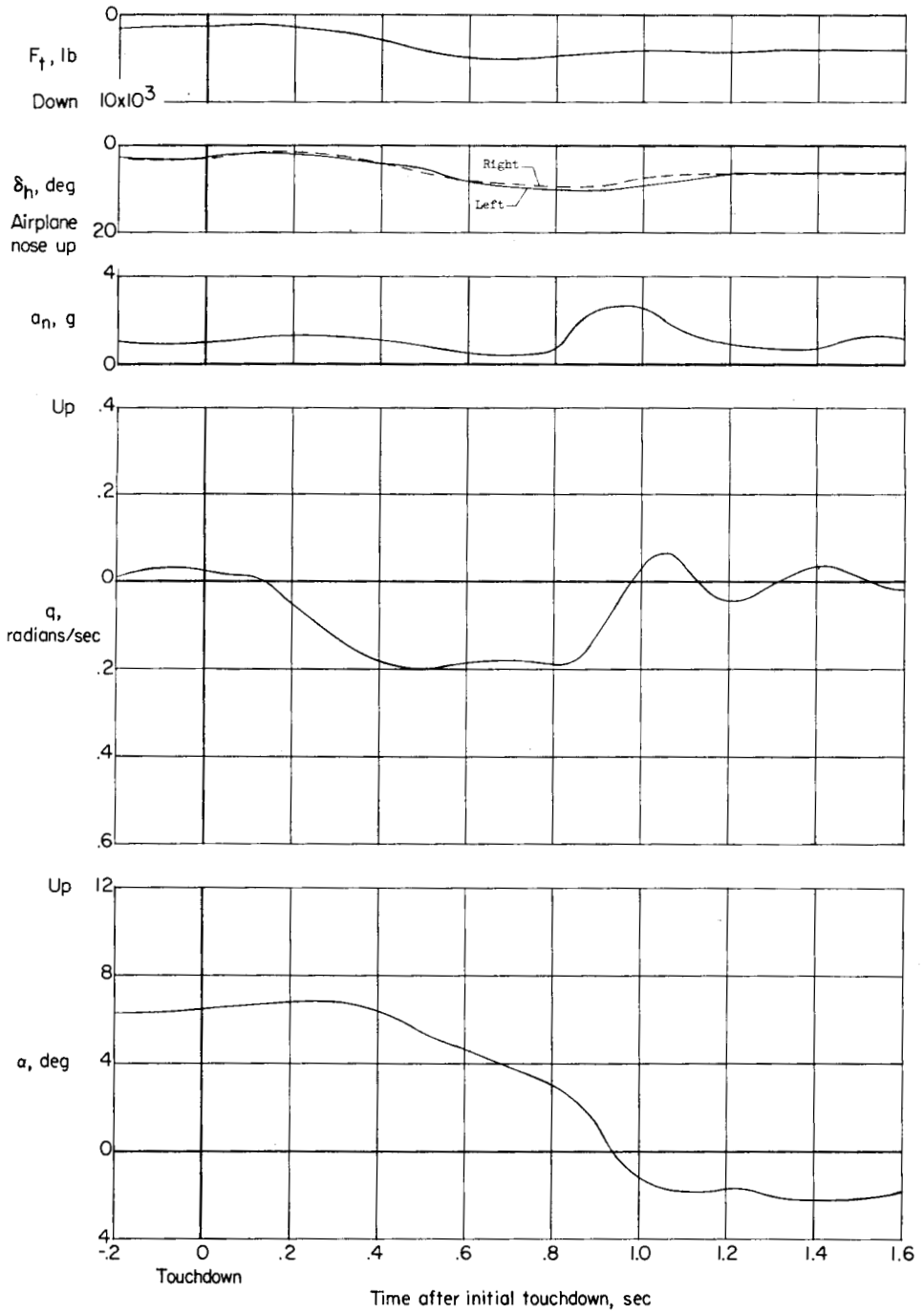

(c) Nose-gear touchdown occurs at $\Delta t_n = 0.795$ second (flight 2-8-16).

Figure 9.- Continued.

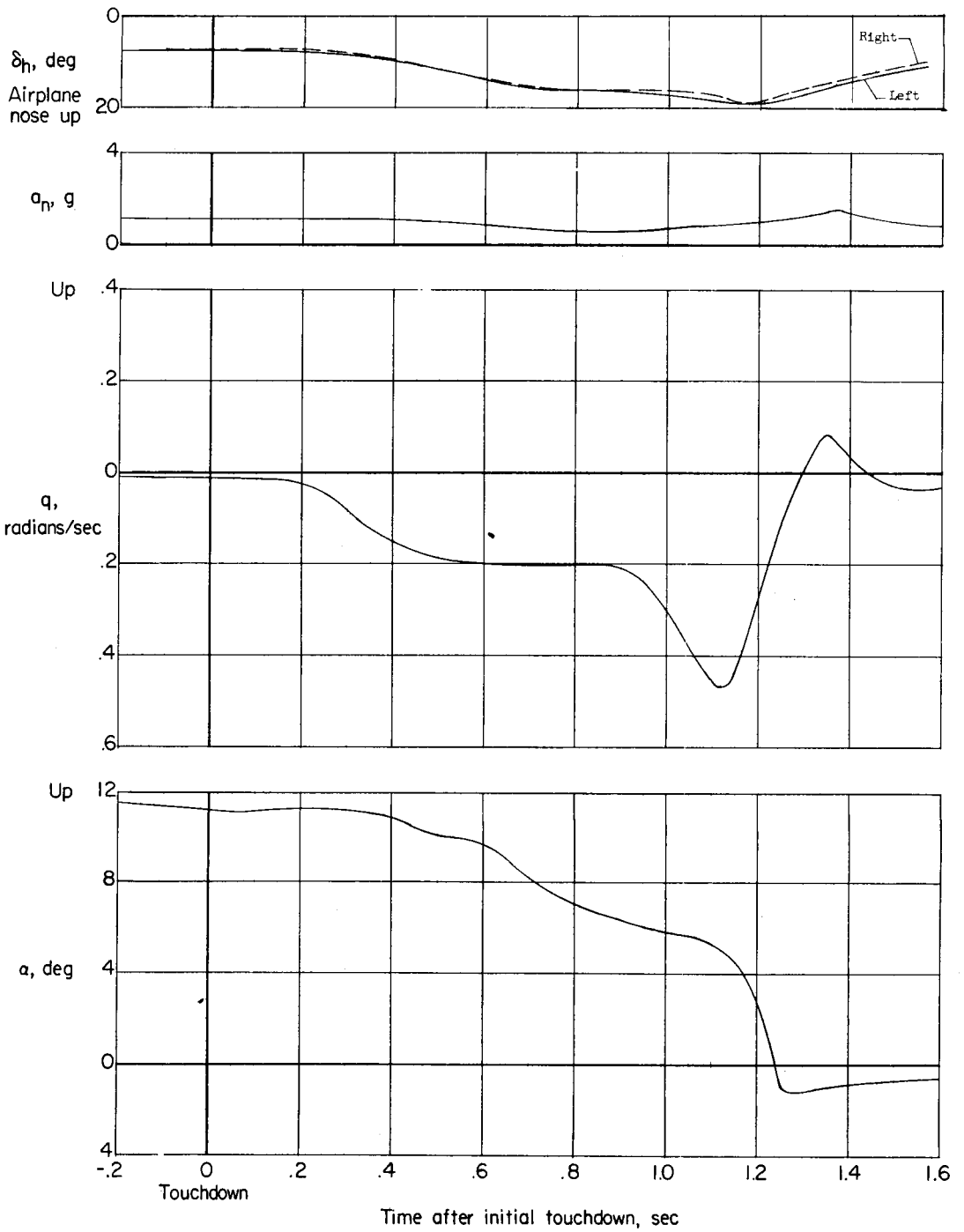

(d) Nose-gear touchdown occurs at Δt_n = 1.090 seconds (flight 2-9-18).

Figure 9.- Concluded.

DECLASSIFIED

CONFIDENTIAL

(a) X-15 airplane. V_v = 6.5 ft/sec (flight 2-4-11). E-5226

Figure 10.- Typical main-gear skid marks on lakebed for the touchdown phase of an X-15 landing.

CONFIDENTIAL

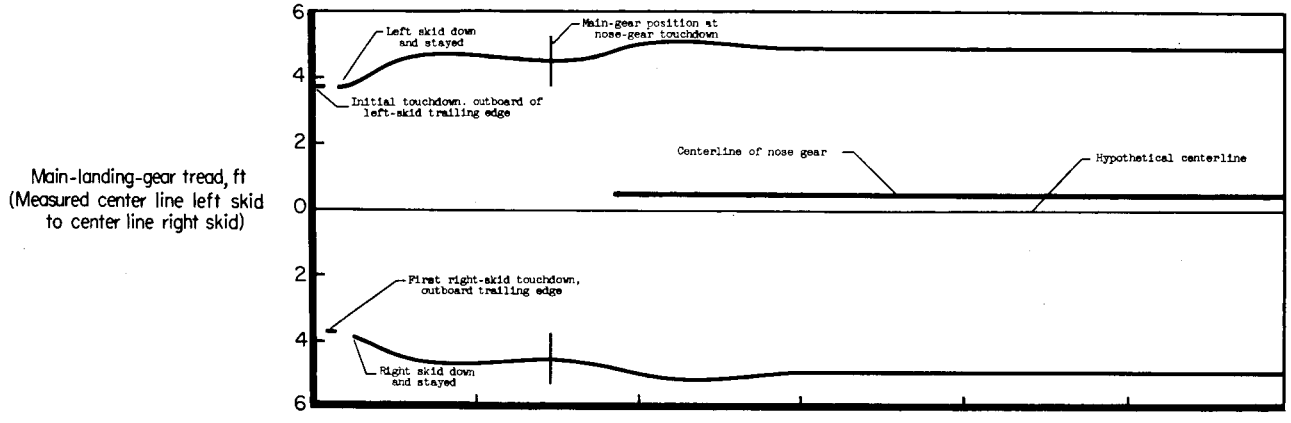

(b) X-15 number 2 airplane. V_V = 6.5 ft/sec (flight 2-4-11).

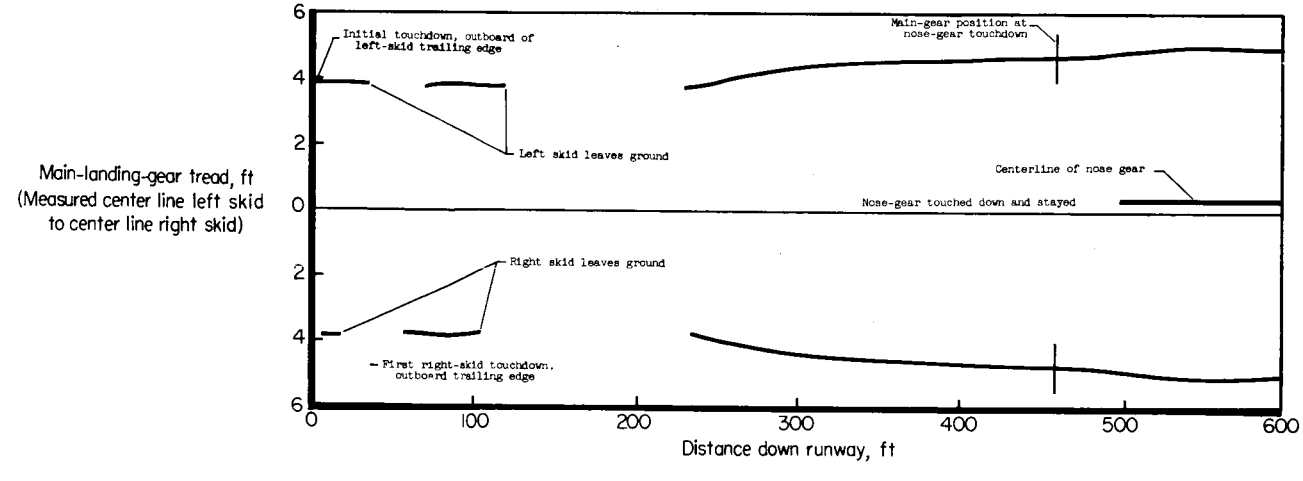

(c) X-15 number 1 airplane. V_V = 1.0 ft/sec (flight 1-6-11).

Figure 10.- Concluded.

UNCLASSIFIED

E-5233

Figure 11.- Landing-gear marks during runout phase illustrating directional stability and lack of nosewheel shimmy of the X-15 airplane (flight 2-4-11).

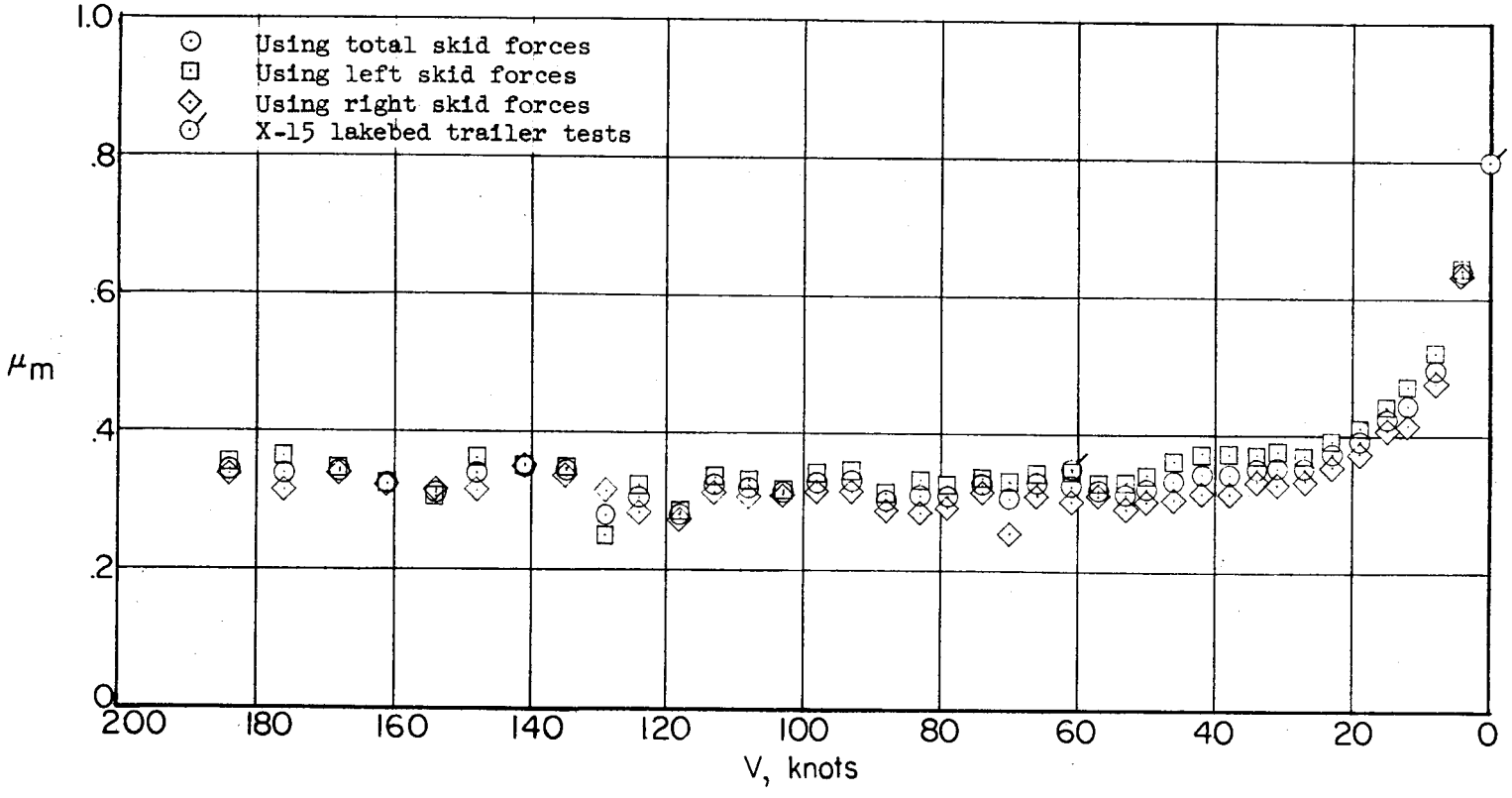

(a) Calculated using F_{h_m} obtained from the main-landing-gear drag-brace loads.

Figure 12.- Variation of coefficient of friction of main-landing-gear skid with true ground speed for the X-15 research airplane.

UNCLASSIFIED

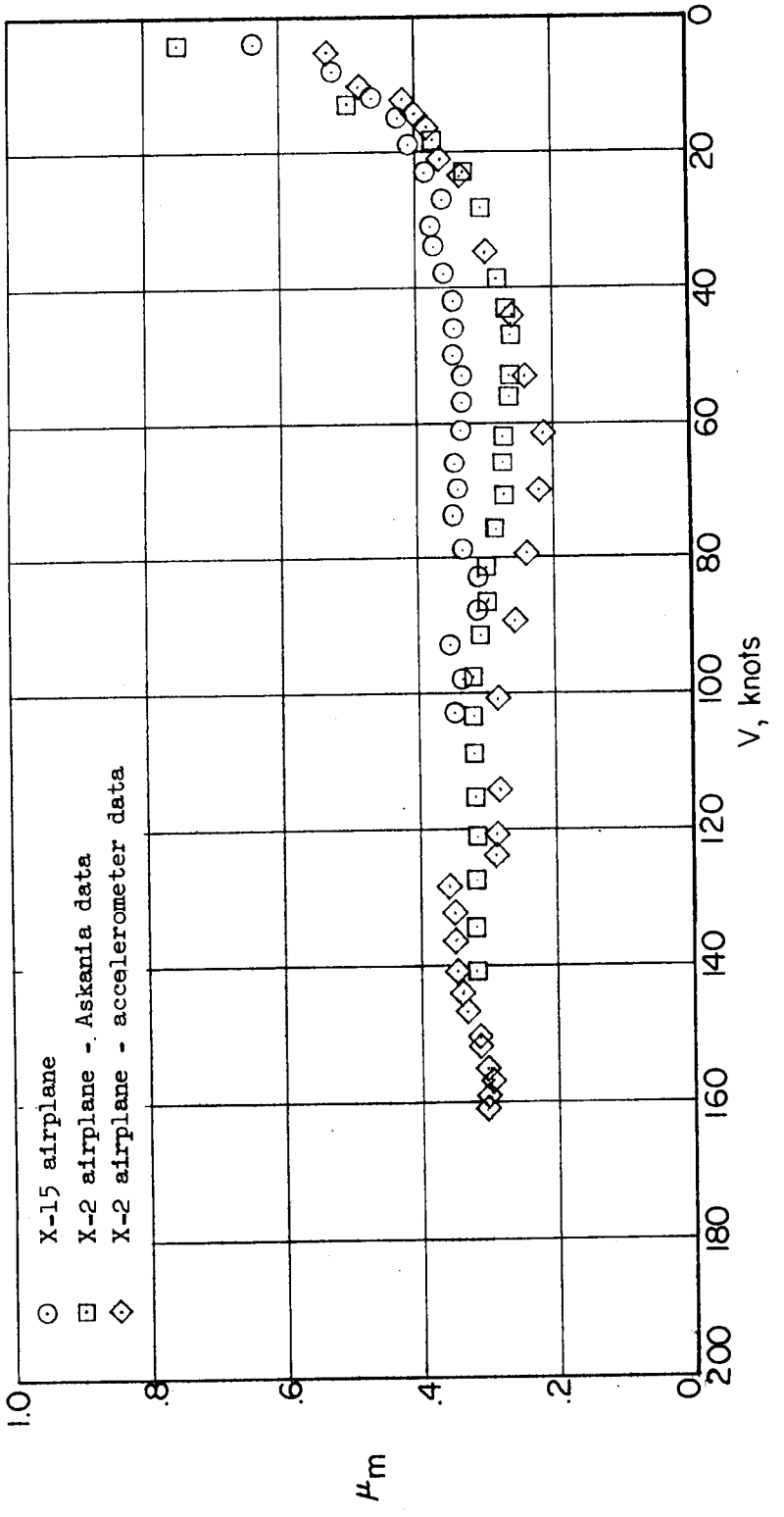

(b) Calculated using $F_{h_m} = W_L a_l - F_{h_n} - D_A$.

Figure 12.- Concluded.

UNCLASSIFIED

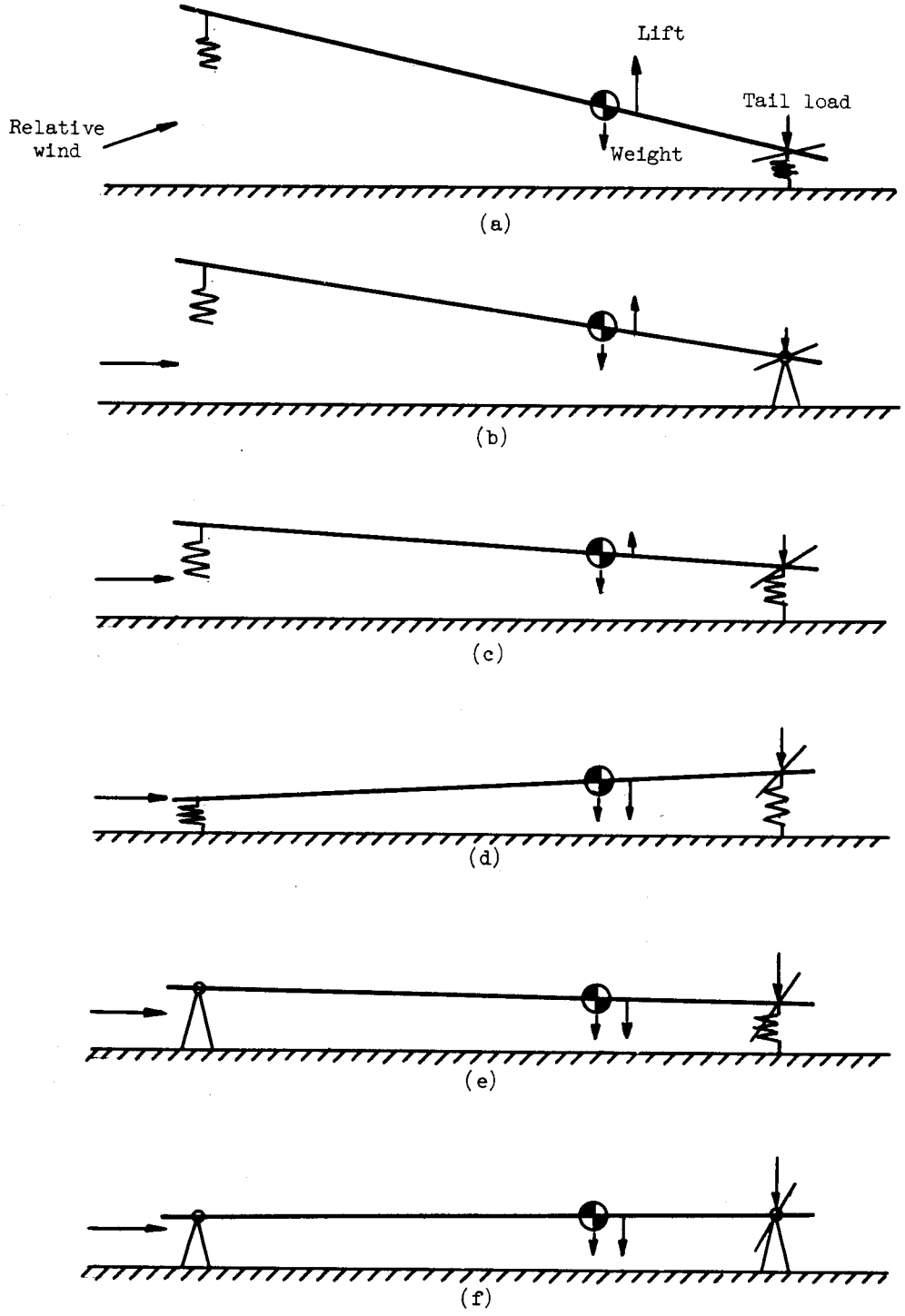

Figure 13.- Landing sequence of X-15 airplane showing conditions leading to second main-gear impact.

UNCLASSIFIED

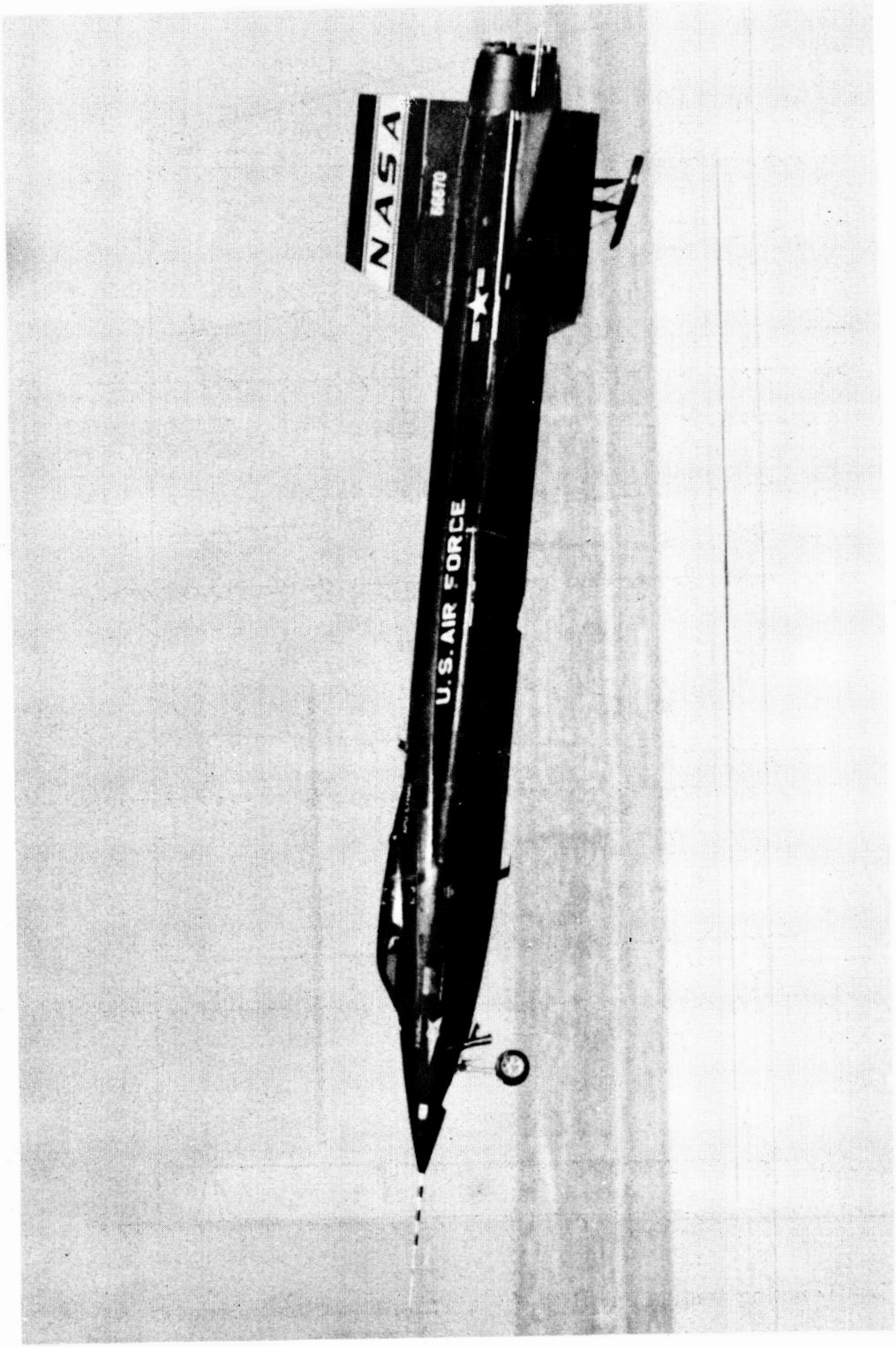

E-6107

Figure 14.- X-15 airplane just prior to touchdown.

UNCLASSIFIED

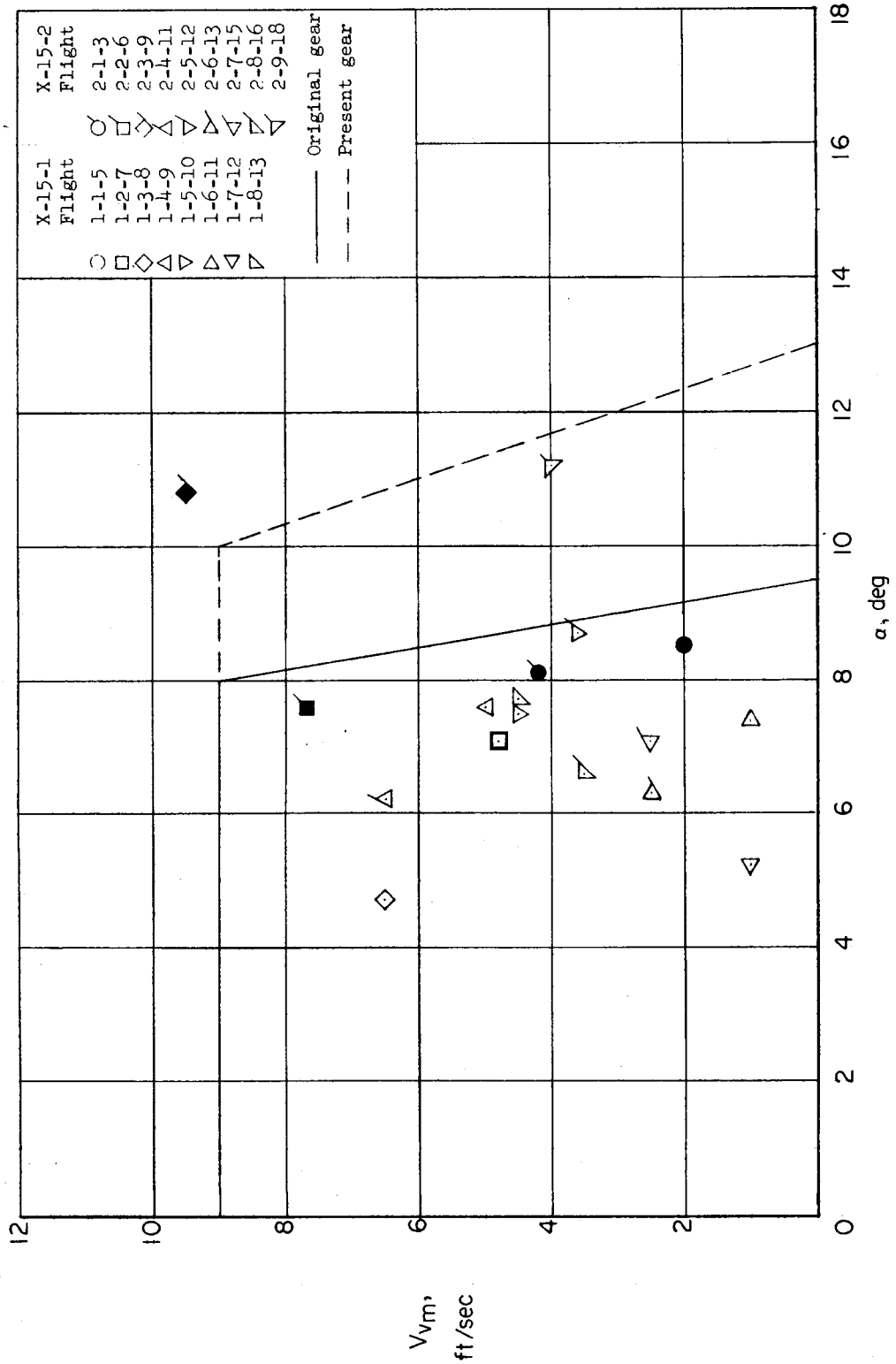

Figure 15.- X-15 design-limit landing envelope for the original and the present landing-gear system. (Solid symbols indicate landings with original gear system.)